


# Nonasymptotic Convergence Rate of Quasi-Monte Carlo: Applications to Linear Elliptic PDEs with Lognormal Coefficients and Importance Samplings

Yang Liu <sup>a,1,\*</sup>, Raúl Tempone <sup>a,1,2</sup>

<sup>a</sup>*Computer, Electrical and Mathematical Sciences and Engineering,  
4700 King Abdullah University of Science and Technology (KAUST),  
Thuwal 23955-6900, Kingdom of Saudi Arabia*

---

## Abstract

This study analyzes the nonasymptotic convergence behavior of the quasi-Monte Carlo (QMC) method with applications to linear elliptic partial differential equations (PDEs) with lognormal coefficients. Building upon the error analysis presented in (Owen, 2006), we derive a nonasymptotic convergence estimate depending on the specific integrands, the input dimensionality, and the finite number of samples used in the QMC quadrature. We discuss the effects of the variance and dimensionality of the input random variable. Then, we apply the QMC method with importance sampling (IS) to approximate deterministic, real-valued, bounded linear functionals that depend on the solution of a linear elliptic PDE with a lognormal diffusivity coefficient in bounded domains of  $\mathbb{R}^d$ , where the random coefficient is modeled as a stationary Gaussian random field parameterized by the trigonometric and wavelet-type basis. We propose two types of IS distributions, analyze their effects on the QMC convergence rate, and observe the improvements.

**Keywords:** Quasi-Monte Carlo, Importance sampling, Finite elements, Partial differential equations with random data, Lognormal diffusion, Wavelets

**2020 MSC:** 65C05, 65N50, 65N22, 35R60


---

## 1. Introduction

The quasi-Monte Carlo (QMC) method computes the expectation of a random variable using deterministic low-discrepancy sequences. The QMC method offers a convergence rate of  $\mathcal{O}(n^{-1+\epsilon})$  for  $\epsilon > 0$ , surpassing the Monte Carlo

---

\*Corresponding author

Email address: [yang.liu.3@kaust.edu.sa](mailto:yang.liu.3@kaust.edu.sa) (Yang Liu )

<sup>1</sup>KAUST SRI Center for Uncertainty Quantification in Computational Science and Engineering

<sup>2</sup>Alexander von Humboldt Professor in Mathematics for Uncertainty Quantification, RWTH Aachen University, 52062 Aachen, Germany

convergence rate of  $\mathcal{O}(n^{-1/2})$ . However, the effectiveness of the QMC method depends on the regularity of the integrand and the integration dimension. The integrand variation and integration dimension dictate the classical upper bound for the QMC method, known as the Koksma–Hlawka inequality [36].

Concerns about the quality of point sets arise as the integration dimension increases [13, 29, 34, 52]. For instance, the Halton sequence may exhibit pathological behavior in certain dimensions; thus, researchers have proposed remedies [12, 42].

Despite these challenges, the QMC method has been successful in relatively high dimensions due to the “low effective dimension” [50, 51]. This notion first arose from the analysis of variance (ANOVA) decomposition in [9]. Several studies have aimed to apply various approaches to minimize the effective dimension, particularly in financial applications [6, 7, 49]. Nevertheless, an equivalence theorem in [53], an extension of the worst-case integration error analysis in [44], stated that no decomposition method (includes Brownian bridge, principal component analysis, etc.) is consistently superior to other methods in terms of different payoff functions. Nonetheless, considering the exact forms of the payoff function, the authors of [24] introduced the linear transformation method, exploiting the nonuniqueness of the covariance matrix decomposition to find the most important dimensions. The design of the transformation matrix’s columns optimizes the variance contribution of each random variable.

In addition to the effective dimension, the regularity of the integrand also affects the QMC integration. In finance applications, option pricing problems can sometimes involve discontinuous functions. The orthogonal transformation was proposed in [54] to transform the discontinuity, involving a linear combination of the random variables, to become parallel to the axes. The authors of [25] discussed the connection between orthogonal and linear transformation methods. The authors in [20] characterized the “QMC-friendly” axis-parallel discontinuity and explicitly derived the convergence rate for integrands with such discontinuities, supported by numerical experiments. Although the optimal QMC convergence rates are not recovered, the superiorities to the MC methods are shown.

Conditioning is a well-known approach to reduce variance, but it can also improve the smoothness [4, 7, 19, 55]. In [18], the authors demonstrated that, under certain conditions, all terms from the ANOVA decomposition except the one with the highest order have infinite smoothness. In addition, in [14], the conditions under which preintegration works were provided. In [31], the authors proposed preintegrating in a subspace comprising a linear combination of random input variables. Moreover, previous studies [5, 26] exploited the regularity with Fourier transformation when the original function exhibits non-smoothness.

A partial differential equation (PDE) with random coefficients is another application in which the QMC method accelerates the convergence of computing the statistical properties of a quantity of interest (QoI), often taking the form of a functional of the PDE solution. In [47], the authors proved that the QMC worst-case error is independent of the dimension if the integrand belongs to a

class of weighted Sobolev spaces. Another study [35] considered the weights of the form “product and order dependent” to minimize the worst-case error and provide a fast method to design the lattices according to the weights. The dimension-independent worst-case QMC errors of elliptic PDEs with affine uniform and lognormal coefficients were analyzed in [30] and [17]. In the latter case, the space is equipped with additional weight functions. Moreover, in [22, 27], the authors considered the “product weights” in the weighted space and lattice rule design. More recent studies [16] and [43] have considered the median-of-the-mean QMC estimator using lattice rule (without specific design) and digital sequence, respectively.

Despite the careful analysis of the asymptotic convergence rates in the literature, the ideal QMC convergence rate  $\mathcal{O}(n^{-1})$  is not always observed in practice. In this work, we aim to study the nonasymptotic convergence behavior of the QMC method and explain the often observed suboptimal convergence rates.

Specifically, certain integration problems involve integrand domains different from  $[0, 1]$ , such as the integration with respect to (w.r.t) the Gaussian measure on  $\mathbb{R}$ . The inverse cumulative distribution function (CDF) transformation is applied for compatibility with QMC methods. However, this transformation often introduces singularities at the boundaries. The work [39] characterized the boundary singularity with the boundary growth rate and made connections with the asymptotic QMC convergence rate. Particularly, the author provided examples of integrands which blow up at boundaries but still lead to optimal QMC convergence rate. Building on this work, we aim to analyze the nonasymptotic QMC convergence rate for some examples involving lognormal random variables to explain the observed suboptimal rates. Last, the importance sampling (IS) is a well-known method for variance reduction. We also aim to discover the extent to which IS with certain proposal distributions improves the convergence rate.

Some recent publications have delved into the realm of QMC methods for potentially unbounded integrands. One study [15] combined the robust mean estimator with QMC sampling. In parallel, the work [21] and [37] studied the QMC method with IS. While these studies provided valuable insights into the asymptotic convergence rate, they did not address the nonasymptotic behaviors frequently observed in real-world scenarios. In contrast, our work contributes to developing a convergence rate model for QMC methods with a finite number of samples. This innovative approach offers potential pathways to enhance the practically-observed convergence rate.

The paper is organized as follows. Section 2 discusses the nonasymptotic convergence rate. Next, Section 3 presents the convergence rate analysis for two examples: the expectation of a lognormal random variable and elliptic PDEs with lognormal coefficients. Then, Section 4 evaluates the effects of two kinds of IS distributions. Section 5 details the numerical results. Finally, Section 6 presents the conclusions.

## 2. Nonasymptotic convergence rate for the randomized QMC method

This section follows the proofs in [39] and accordingly modifies them to establish the nonasymptotic results. First, we introduce the notation. We are interested in the following integration problem:

$$I(g) = \int_{[0,1]^s} g(\mathbf{t}) d\mathbf{t}, \quad (1)$$

where  $g : [0, 1]^s \rightarrow \mathbb{R}$ . We let  $\mathcal{P} = \{\mathbf{t}_1, \mathbf{t}_2, \dots, \mathbf{t}_n\}$  be a point set in  $[0, 1]^s$ .

The QMC estimator for the integrand  $g$  is given by

$$\hat{I}_n(g) = \frac{1}{n} \sum_{i=1}^n g(\mathbf{t}_i), \quad (2)$$

where the  $\{\mathbf{t}_i\}_{i=1}^n$  is a predesigned deterministic low-discrepancy sequence [11, 36]. A notion to describe how well the points in  $\mathcal{P}$  are uniformly distributed is the star discrepancy  $\Delta_{\mathcal{P}}^*$ , given by

$$\Delta_{\mathcal{P}}^* := \sup_{\mathbf{x} \in [0,1]^s} |\Delta_n(\mathbf{x}; \mathcal{P})|, \quad (3)$$

where  $\Delta_n(\mathbf{x}; \mathcal{P}) = \frac{1}{n} \sum_{j=1}^n \mathbb{1}_{\mathbf{t}_j \in [0, \mathbf{x}]} - \prod_{k=1}^s x_k$ , which is the difference of the measure of  $[0, \mathbf{x})$  and the proportion of points that belong to this set, where  $[0, \mathbf{x})$  denotes the tensor product of each dimension, i.e.  $[0, \mathbf{x}) = \prod_{k=1}^s [0, x_k)$ . We expect a small difference for an evenly distributed point set. For some low-discrepancy sequences with fixed length  $n$ , we have

$$\Delta_{\mathcal{P}}^* = \mathcal{O}(n^{-1}(\log n)^s), \quad (4)$$

where the exponent of the log term becomes  $s-1$  for an infinite sequence [11, 36].

In this work we consider functions with a continuous mixed first-order derivative. The variation in the Hardy–Krause sense can be computed as follows:

$$V_{HK}(g) = \sum_{\emptyset \neq \mathbf{u} \subseteq \{1, 2, \dots, s\}} \int_{[0,1]^{|\mathbf{u}|}} |\partial^{\mathbf{u}} g(\mathbf{t}^{\mathbf{u}} : \mathbf{1}^{-\mathbf{u}})| d\mathbf{t}^{\mathbf{u}}, \quad (5)$$

where  $|\mathbf{u}|$  is the cardinality of the set  $\mathbf{u}$ ,  $\mathbf{y} = \mathbf{t}^{\mathbf{u}} : \mathbf{1}^{-\mathbf{u}} \in [0, 1]^s$  denotes a point in  $[0, 1]^s$  with  $y^j = t^j$  for  $j \in \mathbf{u}$ , and  $y^j = 1$  otherwise. For the set  $\mathbf{u} = \{u_1, \dots, u_{|\mathbf{u}|}\} \subseteq \{1, \dots, s\}$ , the mixed derivative  $\partial^{\mathbf{u}} g$  is explicitly given by

$$\partial^{\mathbf{u}} g(\mathbf{t}) = \frac{\partial^{|\mathbf{u}|} g}{\partial \mathbf{t}_{\mathbf{u}}}(\mathbf{t}) = \frac{\partial}{\partial t_{u_{|\mathbf{u}|}}} \cdots \frac{\partial}{\partial t_{u_1}} g(\mathbf{t})$$

where the continuity ensures that the order of differentiation can be switched while maintaining derivative invariance.

The Koksma–Hlawka inequality provides an error estimate for the QMC method, given by

$$\left| I(g) - \hat{I}_n(g) \right| \leq V_{HK}(g) \Delta_{\mathcal{P}}^*, \quad (6)$$

where  $V_{HK}(g)$  is the variation of  $g$  in the Hardy–Krause sense.

However, the use of a deterministic point set yields biased results. Randomization techniques have been introduced to address this problem, giving rise to the randomized QMC (RQMC) unbiased estimator [32]:

$$\hat{I}_{R,n}(g) = \frac{1}{R} \sum_{r=1}^R \frac{1}{n} \sum_{i=1}^n g(\mathbf{t}_i \oplus \mathbf{\Delta}_r) = \frac{1}{R} \sum_{r=1}^R \hat{I}_n^{(r)}(g), \quad (7)$$

where  $\mathbf{t}_i$  is the  $i$ th deterministic QMC quadrature point,  $\mathbf{\Delta}_r$  represents the  $r$ th randomization, and  $\oplus$  denotes the randomization operation. An example of such an operation is the random shift, where  $\mathbf{\Delta}_r$  are i.i.d. sampled from uniform distribution  $U[0, 1]^s$  and  $\mathbf{a} \oplus \mathbf{b} = (\mathbf{a} + \mathbf{b}) \bmod 1$ , with the modulo taken component-wise. This random shift approach is easy to implement and provides an unbiased integral estimator. Apart from the unbiasedness, the randomization also provides an convenient access to the estimator variance.

In this work, we consider specifically the problem of evaluating the integral

$$\begin{aligned} I(g) &= \int_{[0,1]^s} g(\mathbf{t}) d\mathbf{t} \\ &= \int_{\mathbb{R}^s} g \circ \Phi(\mathbf{y}) \rho(\mathbf{y}) d\mathbf{y}, \end{aligned} \quad (8)$$

where  $\circ$  denotes the function composition,  $\mathbf{y} = \Phi^{-1}(\mathbf{t})$ ,  $\Phi^{-1} : [0, 1]^s \rightarrow \mathbb{R}^s$  the inverse CDF of  $s$ -dimensional standard normal distribution, and  $\rho$  represents its probability density function. Section 3 presents two concrete examples of  $g$ . Before we analyze such an integrand, we study the behavior of uniform random variables.

### 2.1. Some properties of the uniform distribution

Lemma 1 introduces a useful property of the uniform distribution.

**Lemma 1** (A bound for an  $s$ -dimensional uniform random variable). *Let each  $\mathbf{t}_i$  in the sequence  $\{\mathbf{t}_i\}_{i=1}^\infty$  be uniformly distributed over  $[0, 1]^s$ . Define  $E_n$  as the event  $\{\prod_{j=1}^s t_n^j \leq C \cdot n^{-r}\}$  for  $r > 1$  and  $C > 0$ . Then, we have*

$$\Pr(E_n \text{ i.o.}) = 0, \quad (9)$$

where *i.o.* stands for “infinitely often.”

The sequence  $\{\mathbf{t}_i\}$  in Lemma 1 is not necessarily independent, as is the case for the RQMC method, where the points are desired to exhibit a negative correlation [56]. Lemma 1 is a slight modification of Lemma 4.1 in [39], where the minimum condition is removed. The proof follows [39], except we corrected an upper bound.

*Proof.* Let  $\mathbf{t}_n \sim U[0, 1]^s$ . We have

$$\begin{aligned}
\Pr \left( \prod_{j=1}^s t_n^j \leq C \cdot n^{-r} \right) &= \Pr \left( -2 \log \left( \prod_{j=1}^s t_n^j \right) \geq 2r \log(n) - 2 \log(C) \right) \\
&= \Pr \left( \chi_{(2s)}^2 \geq 2r \log(n) - 2 \log(C) \right) \\
&= \int_{2r \log(n) - 2 \log(C)}^{\infty} \frac{z^{s-1} e^{-z/2}}{2^s \Gamma(s)} dz \\
&= \int_{r \log(n) - \log(C)}^{\infty} \frac{y^{s-1} e^{-y}}{\Gamma(s)} dy,
\end{aligned} \tag{10}$$

where  $\chi_{(2s)}^2$  denotes a chi-squared distribution with  $2s$  degrees of freedom and  $\Gamma(s)$  denotes the gamma function evaluated at  $s$ . Now, we use the upper bound derived in [46] for the incomplete gamma function:

$$\Gamma(s, x) = \int_x^{\infty} y^{s-1} e^{-y} dy \leq G_s(x) \tag{11}$$

where

$$G_s(x) = \frac{(x + b_s)^s - x^s}{s b_s} e^{-x} \tag{12}$$

with  $b_s = \Gamma(s+1)^{\frac{1}{s-1}}$ . Then, we can bound (10) by

$$\begin{aligned}
\int_{r \log(n) - \log(C)}^{\infty} \frac{y^{s-1} e^{-y}}{\Gamma(s)} dy &\leq \frac{G_s(\log(\frac{n^r}{C}))}{\Gamma(s)} \\
&= \frac{\left( \log\left(\frac{n^r}{C}\right) + \Gamma(s+1)^{\frac{1}{s-1}} \right)^s - \left( \log\left(\frac{n^r}{C}\right) \right)^s}{\Gamma(s) s \Gamma(s+1)^{\frac{1}{s-1}}} \cdot \frac{C}{n^r}.
\end{aligned} \tag{13}$$

The last expression in (13) is summable, for  $n = 1, \dots, +\infty$ , yielding  $\sum_{n=1}^{\infty} \Pr(E_n) < \infty$ . Thus, by the Borel–Cantelli lemma,

$$\begin{aligned}
\Pr(E_n \text{ i.o.}) &= \Pr \left( \bigcap_{n=1}^{\infty} \bigcup_{k=n}^{\infty} E_k \right) \\
&= \lim_{n \rightarrow \infty} \Pr \left( \bigcup_{k=n}^{\infty} E_k \right) \\
&\leq \lim_{n \rightarrow \infty} \sum_{k=n}^{\infty} \Pr(E_k) \\
&= 0.
\end{aligned}$$

□

**Remark 1** (Results in earlier literature). *Lemma 4.1 in [39] states a stronger result, namely that*

$$\Pr \left( \min_{1 \leq i \leq n} \prod_{j=1}^s t_i^j \leq C \cdot n^{-r} \text{ i.o.} \right) = 0. \quad (14)$$

*However, the additional condition*

$$\min_{1 \leq i \leq n}$$

*leads to a conclusion that is different from the statement (14). Specifically, if we assume  $\{\mathbf{t}_i\}_{i=1}^n$  are independently and identically distributed (i.i.d.)  $U[0, 1]^s$  and define the event  $F_n = \{\min_{1 \leq i \leq n} \prod_{j=1}^s t_i^j \leq n^{-r}\}$ . We choose  $C = 1$  for simplicity. Then,*

$$\begin{aligned} \Pr(F_n \text{ i.o.}) &= \Pr \left( \bigcap_{n=1}^{\infty} \bigcup_{k=n}^{\infty} F_k \right) \\ &= \lim_{n \rightarrow \infty} \Pr \left( \bigcup_{k=n}^{\infty} F_k \right) \\ &\geq \lim_{n \rightarrow \infty} \Pr(F_n) \\ &= \lim_{n \rightarrow \infty} \left( 1 - \prod_{i=1}^n \Pr \left( \prod_{j=1}^s t_i^j > n^{-r} \right) \right). \end{aligned}$$

*For example, when  $s = 1$ ,*

$$\begin{aligned} \lim_{n \rightarrow \infty} \left( 1 - \prod_{i=1}^n \Pr(t_i > n^{-r}) \right) &= \lim_{n \rightarrow \infty} (1 - (1 - n^{-r})^n) \\ &= 1 - \exp \left( -\frac{1}{r} \right). \end{aligned}$$

**Remark 2** (The nonunique constant  $C$ ). *The constant  $C$  in Lemma 1 is not determined uniquely. Nevertheless, we retain this constant  $C$  in the estimation model.*

The event  $E_n$ , as defined in the above proof, only occurs finitely many times *almost surely*. The origin is bounded away in this sense. Through symmetry arguments, we can similarly show that all the  $2^s$  corners are bounded away from the following hyperbolic set:

$$K_{n,s} = \left\{ \mathbf{t} \in [0, 1]^s \mid \prod_{1 \leq j \leq s} \min(t_j, 1 - t_j) \geq Cn^{-1} \right\}, \quad (15)$$

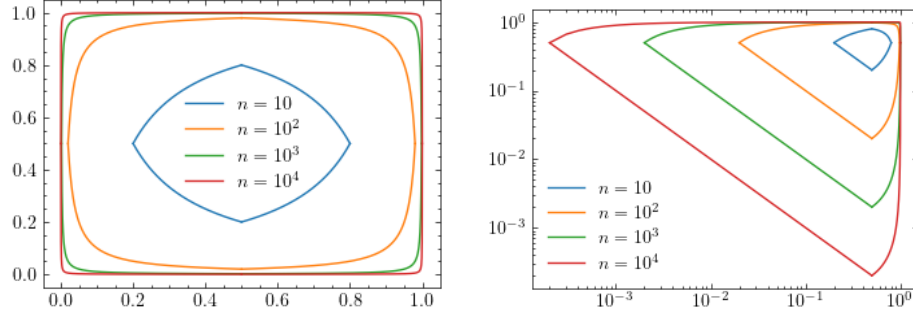


Figure 1: Illustration of the hyperbolic set  $K_{n,s}$  introduced in (15) using the linear scale (left) and log scale (right) for various  $n$ , where  $C = 1$ .

where we use the boundary case  $n^{-1}$  instead of  $n^{-r}$  from Lemma 1. We also set  $Cn^{-1} \leq 1$  to exclude trivial cases.

From Lemma 1, we see that the uniform distribution samples “diffuse” to the corner at a certain rate.

Figure 2 plots the  $n$  samples from the uniform distribution  $U[0,1]^2$  and the corresponding reference boundaries  $t_1 t_2 = n^{-1}$ . The samples approach the corner when size increases and a small portion of samples lie outside their corresponding reference boundaries.

## 2.2. Integrand with infinite variation

We are often interested in integrands with infinite variation, for which the Koksma–Hlawka inequality (6) is not informative. However, cases remain where the QMC methods work. The study [20] considered discontinuities inside the integration domain and proved that the convergence rate is still superior to the Monte Carlo method as long as some axes are parallel to the discontinuity interface. Another study [39] explored integrands that blow up at the boundary of  $[0,1]^s$  and derived convergence rates based on a boundary growth condition. We are interested in the latter case. Following the work [39], the set  $K_{n,s}$  was introduced to split the integration domain and the Sobol’ low-variation extension [48]  $\tilde{g}$  extends  $g$  from  $K_{n,s}$  to  $[0,1]^s$ . The extension  $\tilde{g}$  depends on  $n$  and  $s$  through the hyperbolic set  $K_{n,s}$ , but we suppress these dependences for the sake of simpler notations. Though the original name in the literature states “low-variation”, we assure the readers that the extension  $\tilde{g}$  indeed has finite variation. For completeness, we provide the details here.

To this end, some notations need to be introduced. For an index set  $\mathbf{u} \subseteq \{1, 2, \dots, s\}$ ,  $-\mathbf{u}$  denotes its complement  $\{1, 2, \dots, s\} \setminus \mathbf{u}$ . The notation  $\mathbf{z}^{\mathbf{u}} : \mathbf{c}^{-\mathbf{u}}$  is used to denote the point  $\mathbf{y} \in [0,1]^s$ , where  $y^j = z^j$  for  $j \in \mathbf{u}$  and  $y^j = c^j$  for  $j \notin \mathbf{u}$ , “concatenating” the vectors  $\mathbf{z}^{\mathbf{u}}$  and  $\mathbf{c}^{-\mathbf{u}}$ . For simplicity, we assume the derivative of the integrand  $\partial^{\mathbf{u}} g$  exists in  $(0,1)^s$ , for  $\mathbf{u} \subseteq \{1, 2, \dots, s\}$ . Given an anchor point  $\mathbf{c} \in K_{n,s}$  and using the fundamental theorem of calculus, we



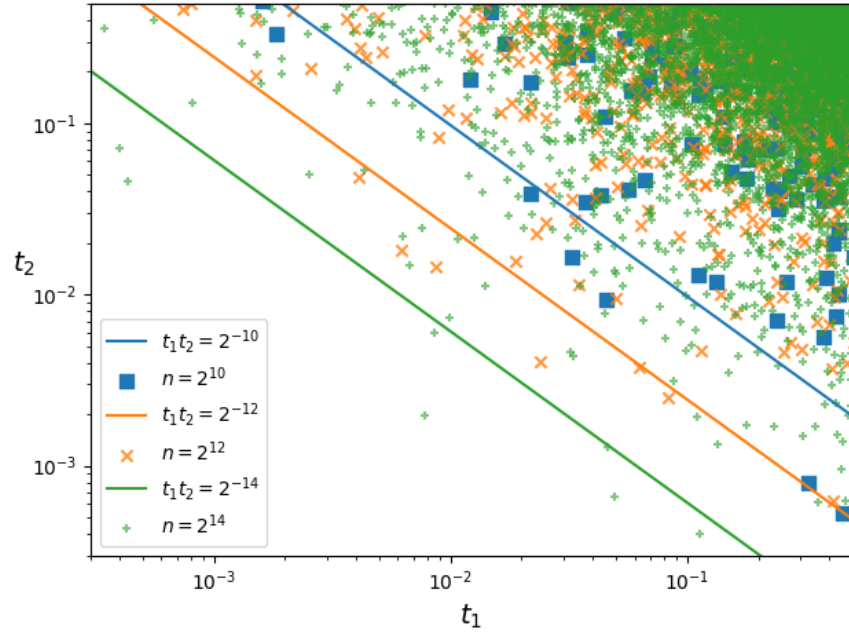


Figure 2: Samples from a two-dimensional uniform distribution  $U[0, 1]^2$  with various sample sizes  $n$ , and the corresponding reference boundaries  $t_1 t_2 = n^{-1}$ .

obtain

$$g(\mathbf{t}) = g(\mathbf{c}) + \sum_{\mathbf{u} \neq \emptyset} \int_{[\mathbf{c}^{\mathbf{u}}, \mathbf{t}^{\mathbf{u}}]} \partial^{\mathbf{u}} g(\mathbf{z}^{\mathbf{u}} : \mathbf{c}^{-\mathbf{u}}) d\mathbf{z}^{\mathbf{u}}. \quad (16)$$

The Sobol' low-variation extension  $\tilde{g} : \mathbb{R}^s \rightarrow \mathbb{R}$  is given by

$$\tilde{g}(\mathbf{t}) = g(\mathbf{c}) + \sum_{\mathbf{u} \neq \emptyset} \int_{[\mathbf{c}^{\mathbf{u}}, \mathbf{t}^{\mathbf{u}}]} \mathbb{1}_{\{\mathbf{z}^{\mathbf{u}} : \mathbf{c}^{-\mathbf{u}} \in K_{n,s}\}} \partial^{\mathbf{u}} g(\mathbf{z}^{\mathbf{u}} : \mathbf{c}^{-\mathbf{u}}) d\mathbf{z}^{\mathbf{u}}. \quad (17)$$

Following [39, 48], we apply a three-epsilon argument to bound the integration error. Recalling the notations on the exact integration (1) and QMC estimation (2), we bound:

$$\begin{aligned} |I(g) - \hat{I}_n(g)| &\leq |I(g) - I(\tilde{g})| + |I(\tilde{g}) - \hat{I}_n(\tilde{g})| + |\hat{I}_n(\tilde{g}) - \hat{I}_n(g)| \\ &\leq \int_{[0,1]^s - K_{n,s}} |g - \tilde{g}| + \Delta^*(\mathbf{t}_1, \dots, \mathbf{t}_n) V_{HK}(\tilde{g}) + \frac{1}{n} \sum_{i=1}^n |\tilde{g}(\mathbf{t}_i) - g(\mathbf{t}_i)|. \end{aligned} \quad (18)$$

Observe that  $g$  and  $\tilde{g}$  coincide in  $K_{n,s}$ . Moreover, we have

$$\begin{aligned} \mathbb{E} \left[ \frac{1}{n} \sum_{i=1}^n |\tilde{g}(\mathbf{t}_i) - g(\mathbf{t}_i)| \right] &= \frac{1}{n} \sum_{i=1}^n \mathbb{E} [|\tilde{g}(\mathbf{t}_i) - g(\mathbf{t}_i)|] \\ &= \int_{[0,1]^s - K_{n,s}} |g - \tilde{g}|. \end{aligned} \quad (19)$$

Using the above inequalities, we obtain the following finite upper bound for the RQMC method:

$$\mathbb{E}[|I(g) - \hat{I}_n(g)|] \leq 2 \int_{[0,1]^s - K_{n,s}} |g - \tilde{g}| + \mathbb{E}[\Delta^*(\mathbf{t}_1, \dots, \mathbf{t}_n)] V_{HK}(\tilde{g}). \quad (20)$$

Notice that the above bound (20) depends on the value of  $C$ , which is used to construct the set  $K_{n,s}$  in Equation (15). When  $C = 0$ , this becomes the classical Koksma–Hlawka inequality, and when  $C = \frac{n}{2^s}$ , the hyperbolic set  $K_{n,s}$  vanishes and the right hand side becomes  $2 \int_{[0,1]^s} |g|$ . For  $0 < C < \frac{n}{2^s}$ , the asymptotic upper bound also reduces to the Koksma–Hlawka inequality, as  $n \rightarrow \infty$ .

To examine the behavior of the difference  $g - \tilde{g}$  and the variation  $V_{HK}(\tilde{g})$  as the set  $K_{n,s}$  grows when  $n$  increases, we assume the following boundary growth condition (in the nonasymptotic case) outside the set  $K_{n,s}$ .

**Assumption 1** (Nonasymptotic boundary growth condition). *For the integrand  $g$ , we assume the following boundary growth condition (21)*

$$|\partial^{\mathbf{u}} g(\mathbf{t})| \leq B(\mathbf{t}_{\mathbf{c}}) \prod_{j=1}^s t_j^{-A_j(t_{\mathbf{c}}^j) - \mathbb{1}_{j \in \mathbf{u}}} \quad \mathbf{0} < \mathbf{t} \leq \mathbf{t}_{\mathbf{c}}, \quad \mathbf{t}_{\mathbf{c}} \in \partial K_{n,s}, \quad (21)$$

for a given constant  $B(\mathbf{t}_{\mathbf{c}})$ ,  $\forall \mathbf{u} \subseteq \{1, 2, \dots, s\}$  and  $A_j < 1/2, \forall j \in \{1, 2, \dots, s\}$ . The inequality  $\mathbf{0} < \mathbf{t} \leq \mathbf{t}_{\mathbf{c}}$  holds component-wise.

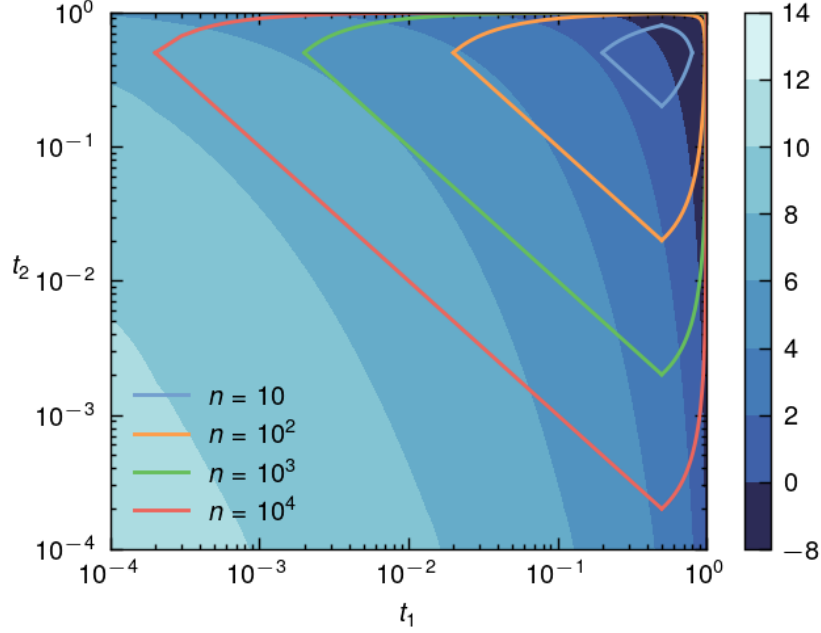


Figure 3: Illustration of the set  $K_{n,s}$  in linear scale with  $C = 1$  and a contour plot of the function  $g(\mathbf{t}) = \exp(2\Phi^{-1}(1 - t_1) + \Phi^{-1}(1 - t_2))$  in log scale.

In Assumption 1, we emphasize the dependence  $A_j = A_j(\mathbf{t}_c)$ , which is crucial in the following nonasymptotic analysis. For now, we consider an anisotropic integrand.

**Example 1** (An anisotropic integrand).

$$g(\mathbf{t}) = \exp(2\Phi^{-1}(1 - t_1) + \Phi^{-1}(1 - t_2)) \quad \mathbf{t} \in [0, 1]^2. \quad (22)$$

As is often the case, the function 22 in our example is not isotropic w.r.t. the coordinates. Figure 3 provides an illustration of the sets  $K_{n,s}$  with  $s = 2$  and the contour of the function 22 on the log scale. The value of  $|\partial^u g(\mathbf{t})|$  may not be constant for  $\mathbf{t} \in \partial K_{n,s}$ .

This finding motivates the determination of an upper bound of the following term:

$$\prod_{j=1}^s t_c^j - A_j(t_c^j), \text{ where } \mathbf{t}_c \in \partial K_{n,s}$$

in dimension  $s > 1$ , which is equivalent to the following optimization problem:

$$\begin{aligned} \max_{\mathbf{t}_c} \quad & \sum_{j=1}^s -A_j \log t_c^j \\ \text{s.t.} \quad & \sum_{j=1}^s \log t_c^j = \log \delta, \end{aligned} \quad (23)$$

for a given  $\delta = Cn^{-1} > 0$ . We define  $\mathbf{t}_c^*$  as the optimizer of (23) and

$$A_j^* = A_j(\mathbf{t}_c^*), \quad (24)$$

for  $j = 1, \dots, s$ . In one dimension, the point  $\mathbf{t}_c^*$  is explicitly given by  $Cn^{-1}$ . For  $s \geq 2$ , and  $\mathbf{t}_c^*$  is determined by solving the optimization problem (23).

Following the proof of Lemma 5.1 in [39], for an integrand  $g$  satisfying the boundary growth condition (21), the difference of the integrand  $g$  and its Sobol' low-variation extension  $\tilde{g}$  is bounded by

$$|g(\mathbf{t}) - \tilde{g}(\mathbf{t})| \leq \tilde{B}(\mathbf{t}_c) \prod_{j=1}^s t_j^{-A_j(t_c^j)} \quad 0 \leq \mathbf{t} \leq \mathbf{t}_c, \quad \mathbf{t}_c \in \partial K_{n,s}, \quad (25)$$

where  $\tilde{B}(\mathbf{t}_c) = B \prod_{j=1}^s (1 + \frac{1}{A_j(t_c^j)})$ . Notice that the power  $-A_j$  has a dependence on the specific choice of  $\mathbf{t}_c \in K_{n,s}$ . Consider the optimization problem (23), we further consider the bound of  $|g - \tilde{g}|$  with the only dependence on  $K_{n,s}$  in Lemma 2.

**Lemma 2** (A bound for the difference of the integrand and its Sobol' low-variation extension). *Let  $\mathbf{t} \notin K_{n,s}$ , for integrand  $g$  satisfying the boundary growth condition (21), we have*

$$|g(\mathbf{t}) - \tilde{g}(\mathbf{t})| \leq \tilde{B}(\mathbf{t}_c^*) \prod_{j=1}^s t_j^{-A_j^*}, \quad (26)$$

where  $A_j^*$  is determined by the optimization problem (23).

*Proof.* Directly using Equation (23) and (25) leads to the result.  $\square$

From Lemma 2, following Lemma 5.4 and the proof of Theorem 5.5 in [39], we have

$$\int_{[0,1]^s - K_{n,s}} |g - \tilde{g}| \leq B_1 n^{\max_j A_j^* - 1}, \quad (27)$$

and

$$V_{HK}(\tilde{g}) \leq B_2 n^{\max_j A_j^*}, \quad (28)$$

for finite  $B_1$  and  $B_2$ . Now, we have obtained the ingredients to present the nonasymptotic upper bound for the RQMC upper bound.

**Theorem 3** (Nonasymptotic QMC error estimate). *For a continuous integrand  $g$  on  $[0, 1]^s$ , whose mixed first-order derivative exists, the expected integration for the RQMC method with a quadrature size of  $n$  satisfies*

$$\mathbb{E}[|I(g) - \hat{I}_n(g)|] \leq C_1 n^{-1+\max_j A_j^*} + C_2 n^{-1+\epsilon+\max_j A_j^*} \quad (29)$$

where  $\epsilon > 0$ , and  $C_1$  and  $C_2$  are finite constants that depend on  $g$  and  $s$ .

*Proof.* Substitute Equation (27) and Equation (28) into (20) and notice that, for low-discrepancy sequences,

$$\mathbb{E}[\Delta^*(\mathbf{t}_1, \dots, \mathbf{t}_n)] = \mathcal{O}(n^{-1}(\log n)^s) \quad (30)$$

(see [41], for reference).  $\square$

Theorem 3 is the contribution of this work to the nonasymptotic QMC error estimate model. We observe that the convergence rate of the RQMC method depends on  $\max_j A_j^*$ , which depends on the QMC quadrature size  $n$ .

**Remark 3** (Nonasymptotics rather than singularity). *In some cases, for instances, the two examples considered in the next Section 3, both integrands exhibit singularities at the boundary. However, the value of  $A_j^*$  from (24) converges to 0 as  $n \rightarrow \infty$ . In this situation, the convergence rate for the RQMC method becomes the optimal asymptotic rate  $\mathcal{O}(n^{-1+\epsilon})$  for  $\epsilon > 0$ , in the presence of the singularities and hence infinite variations. However, the optimal convergence rate may not be observed for a finite sample size  $n$ , as  $A_j^*$  may not converge to 0, resulting a suboptimal convergence rate indicated by Theorem 3. The next section illustrates the nonasymptotics with two concrete examples.*

### 3. Two examples of infinite variation integrands

This section delves into two typical integration examples: the expectation estimate of lognormal random variables and the QoIs relating to the solution of elliptic PDEs with lognormal coefficients. These examples shed light on the intricate nature of infinite variation integrands.

#### 3.1. Lognormal random variable

We first analyze the integration problem (1), where  $g = \exp(\boldsymbol{\sigma}^T \Phi^{-1})$ ,  $\boldsymbol{\sigma} \in \mathbb{R}_+^s$ , and  $\Phi^{-1} : [0, 1]^s \rightarrow \mathbb{R}^s$  applies the inverse standard normal distribution CDF component-wise. The partial derivative of  $g$  w.r.t.  $\mathbf{t}_u$  is given by

$$\begin{aligned} \frac{\partial g}{\partial \mathbf{t}_u} &= \frac{\partial}{\partial \mathbf{t}_u} \exp \left( \sum_{j=1}^s \sigma_j \Phi^{-1}(t_j) \right) \\ &= \exp \left( \sum_{j=1}^s \sigma_j \Phi^{-1}(t_j) \right) \cdot \prod_{j \in u} \sigma_j \partial^j \Phi^{-1}(t_j). \end{aligned} \quad (31)$$

Next, we consider the case where  $t_j \rightarrow 0$  for  $j = 1, \dots, s$ . We use the following approximation:

$$\begin{aligned}\Phi^{-1}(t_j) &= -\sqrt{-2 \log t_j} + o(1) \quad t \rightarrow 0 \\ &\approx -\sqrt{-2 \log t_j}.\end{aligned}\tag{32}$$

The case where  $t_j \rightarrow 1$  can be derived similarly due to symmetry:

$$\Phi^{-1}(t_j) \approx \sqrt{-2 \log(1 - t_j)} \quad t_j \rightarrow 1\tag{33}$$

(see [45], Chapter 3.9, for instance).

Using the approximation of  $\Phi^{-1}$  (33), we can simplify the partial derivative of  $g$  as

$$\begin{aligned}\frac{\partial g}{\partial \mathbf{t}_u} &= \exp \left( \sum_{j=1}^s \sigma_j \Phi^{-1}(t_j) \right) \cdot \prod_{j \in u} \sigma_j \partial^j \Phi^{-1}(t_j) \\ &\approx \exp \left( \sum_{j=1}^s \sigma_j \sqrt{-2 \log(1 - t_j)} \right) \cdot \prod_{j \in u} \sigma_j \partial^j \sqrt{-2 \log(1 - t_j)} \\ &= \exp \left( \sum_{j=1}^s \sigma_j \sqrt{-2 \log(1 - t_j)} \right) \cdot \prod_{j \in u} \sigma_j \frac{1}{(1 - t_j) \sqrt{-2 \log(1 - t_j)}}.\end{aligned}\tag{34}$$

We define  $\mathbf{v} = \mathbf{1} - \mathbf{t}$  to simplify the notation, and the term  $\frac{1}{(1-t)\sqrt{-2 \log(1-t)}}$  behaves like  $\mathcal{O}(v^{-1+\epsilon})$  for any  $\epsilon > 0$  as  $v \rightarrow 0$ . To check the boundary growth condition (21), it remains to study the local growth behavior of the term

$$h(\mathbf{v}) := \exp \left( \sum_{j=1}^s \sigma_j \sqrt{-2 \log v_j} \right) = \exp \left( \sum_{j=1}^s \sigma_j \sqrt{-2 \log(1 - t_j)} \right).\tag{35}$$

**Lemma 4** (First-order Taylor approximation). *The function  $h(\mathbf{v})$  satisfies the following bound:*

$$h(\mathbf{v}) \leq B(\mathbf{v}_c) \prod_{j=1}^s (v_j)^{-A_j} \quad \mathbf{v} \notin K_{n,s},\tag{36}$$

where  $A_j = \frac{\sigma_j}{\sqrt{-2 \log v_c^j}}$ ,  $\mathbf{v}_c \in \partial K_{n,s}$ .

*Proof.* We take the logarithm of  $h(\mathbf{v})$ :

$$\log h(\mathbf{v}) = \sum_{j=1}^s \sigma_j \sqrt{-2 \log(v_j)}.\tag{37}$$

We further apply the change of variable to simplify the notation. For  $\mathbf{v}_c \in \partial K_{n,s}$ , let  $\mathbf{z} = -\log \mathbf{v}$ , and  $\mathbf{z}_c = -\log \mathbf{v}_c$ . By a first-order Taylor approximation of (37),

$$\begin{aligned} \sum_{j=1}^s \sigma_j \sqrt{-2 \log(v_j)} &= \sum_{j=1}^s \sigma_j \sqrt{2z_j} \\ &\leq \nabla_{\mathbf{z}=\mathbf{z}_c} \left( \sum_{j=1}^s \sigma_j \sqrt{2z_j} \right) \cdot (\mathbf{z} - \mathbf{z}_c) + \left( \sum_{j=1}^s \sigma_j \sqrt{2z_c^j} \right) \quad (38) \\ &= \sum_{j=1}^s \frac{\sigma_j}{\sqrt{2z_c^j}} z^j + \sum_{j=1}^s \sigma_j \sqrt{\frac{z_c^j}{2}} \end{aligned}$$

where we use the convexity. By taking the exponential of (38) and comparing with the Equation (36), we deduce that

$$A_j = \frac{\sigma_j}{\sqrt{2z_c^j}} = \frac{\sigma_j}{\sqrt{-2 \log v_c^j}} = \frac{\sigma_j}{\sqrt{-2 \log(1 - t_c^j)}} \quad (39)$$

$$B(\mathbf{v}_c) = \prod_{j=1}^s \exp \left( \sigma_j \sqrt{\frac{-\log(1 - t_c^j)}{2}} \right). \quad (40)$$

□

Notice that  $A_j \rightarrow 0$  as  $t_c^j \rightarrow 1$  for  $j = 1, \dots, s$ . Theorem 3 indicates that the QMC method achieves the asymptotic convergence rate  $\mathcal{O}(n^{-1+\epsilon})$ .

Let us now consider the optimization problem (23):

$$\begin{aligned} \max_{\mathbf{v}_c} \quad & \sum_{j=1}^s -A_j \log v_c^j \\ \text{s.t.} \quad & -\sum_{j=1}^s \log v_c^j = \log \delta^{-1}, \end{aligned} \quad (41)$$

for a given  $\delta = Cn^{-1}$ . The Lagrangian is given by

$$\begin{aligned} \mathcal{L} &= \sum_{j=1}^s -A_j \log v_c^j + \lambda \left( \sum_{j=1}^s -\log v_c^j - \log \delta^{-1} \right) \\ &= \sum_{j=1}^s \sigma_j \sqrt{\frac{-\log v_c^j}{2}} + \lambda \left( \sum_{j=1}^s -\log v_c^j - \log \delta^{-1} \right). \end{aligned} \quad (42)$$

The optimizer  $-\log v_c^{j*}$  for Equation (41) is given by

$$-\log v_c^{j*} = \frac{\sigma_j^2}{\sum_{k=1}^s \sigma_k^2} \log \delta^{-1}. \quad (43)$$

Moreover, the optimal value of  $A_j$ , denoted by  $A_j^*$ , is given by

$$A_j^* = \sqrt{\frac{\sum_{j=1}^s \sigma_j^2}{2 \log \delta^{-1}}} = \sqrt{\frac{\sum_{j=1}^s \sigma_j^2}{2(\log n - \log C)}}. \quad (44)$$

Hence,  $\max_j A_j^* = \sqrt{\frac{\sum_{j=1}^s \sigma_j^2}{2(\log n - \log C)}}$ . For a finite sample size  $n$ , considering the convergence model (29) in Theorem 3, the convergence rate improves as  $n$  increases, or the variance  $\sigma_j^2$  decreases for each dimension  $j$ .

### 3.2. Elliptic partial differential equations with lognormal coefficients

We consider an elliptic PDE on a Lipschitz domain  $\mathcal{D} \in \mathbb{R}^d$ , in the following form:

$$-\nabla_{\mathbf{x}} \cdot (a(\mathbf{x}; \omega) \nabla_{\mathbf{x}} u(\mathbf{x}; \omega)) = f(\mathbf{x}; \omega) \quad \text{for } \mathbf{x} \in \mathcal{D}, \quad (45a)$$

$$u(\mathbf{x}; \omega) = 0 \quad \text{for } \mathbf{x} \in \partial \mathcal{D}, \quad (45b)$$

with almost all  $\omega \in \Omega$ , where  $\Omega$  belongs to a complete probability space tuple  $(\Omega, \mathcal{F}, \mathbb{P})$ . The differential operators  $\nabla \cdot$  and  $\nabla$  are taken w.r.t. the spatial variable  $\mathbf{x}$ , and  $\partial_n$  is the outward normal derivative operator. We explore the equations in (45) in the weak form. For a suitable functional space  $V$  (e.g.,  $V = H_0^1(\mathcal{D})$ ), we seek  $u(\mathbf{x}; \omega) \in V$  such that

$$\langle a(\mathbf{x}; \omega) \nabla_{\mathbf{x}} u(\mathbf{x}; \omega), \nabla_{\mathbf{x}} v(\mathbf{x}; \omega) \rangle = \langle f(\mathbf{x}; \omega), v(\mathbf{x}; \omega) \rangle \quad (46)$$

for all  $v \in V$  and almost all  $\omega \in \Omega$ ,

where  $\langle \cdot, \cdot \rangle$  denotes the inner product. The QoI  $Q(\omega)$  is given in the following general form:

$$Q(\mathbf{y}(\omega)) = \mathcal{G}(u(\cdot; \omega)), \quad (47)$$

where  $\mathcal{G} \in V'$ ,  $V'$  denotes the dual space of  $V$ . We are interested in computing  $\mathbb{E}[Q]$ . The integrand in (1) is given by  $g = Q \circ \Phi^{-1}$ .

We consider  $a(\mathbf{x}; \omega)$ , which takes the following form:

$$a(\mathbf{x}; \omega) = \exp \left( \sum_{j=1}^s y_j \psi_j \right), \quad (48)$$

with  $s \in \mathbb{N}^+$  and  $y_j$  are i.i.d. samples from  $\mathcal{N}(0, 1)$ ,  $j = 1, \dots, s$ . Moreover, we define  $b_j = \|\psi_j\|_{L^\infty(\mathcal{D})} < +\infty$ , for  $j = 1, \dots, s$ .

From [17], an upper bound for the derivative of  $Q$  w.r.t. the random variable  $\mathbf{y}$  is given by

$$\begin{aligned} |\partial^{\mathbf{u}} Q(\mathbf{y})| &\leq \|\mathcal{G}\|_{V'} \|\partial^{\mathbf{u}} u(\cdot, \mathbf{y})\|_V \\ &\leq \frac{|\mathbf{u}|!}{(\ln 2)^{|\mathbf{u}|}} \left( \prod_{j \in \mathbf{u}} b_j \right) \underbrace{\|f\|_{V'} \|\mathcal{G}\|_{V'}}_{K^*} \prod_{j=1}^s \exp(b_j |y_j|) \end{aligned} \quad (49)$$



The derivative of the integrand  $g$  is as follows:

$$\begin{aligned}
|\partial^{\mathbf{u}} g(\mathbf{t})| &= |\partial^{\mathbf{u}} Q(\Phi^{-1}(\mathbf{t}))| = |\partial^{\mathbf{u}} Q| \cdot \prod_{j \in \mathbf{u}} |\partial^j \Phi^{-1}(t_j)| \\
&\leq K^* \frac{|\mathbf{u}|!}{(\ln 2)^{|\mathbf{u}|}} \left( \prod_{j \in \mathbf{u}} b_j \right) \cdot \prod_{j=1}^s \exp(b_j |y_j|) |\partial^j \Phi^{-1}(t_j)| \\
&\approx K^* \frac{|\mathbf{u}|!}{(\ln 2)^{|\mathbf{u}|}} \left( \prod_{j \in \mathbf{u}} b_j \right) \prod_{j=1}^s b_j \exp\left(b_j \sqrt{-2 \log(t_j)}\right) \cdot \prod_{j=1}^s \frac{1}{t_j \sqrt{-2 \log(t_j)}},
\end{aligned} \tag{50}$$

where we apply the approximation of  $\Phi^{-1}$  (32) as  $t_j$  approaches 0, where  $j = 1, \dots, s$ . Unlike the example in Section 3.1, the considered integrand  $g$  has singularities when  $t_j \rightarrow 0$  and  $t_j \rightarrow 1$ . Due to the symmetry in each dimension, we only need to consider the singularity at 0. To investigate the local growth behavior of the derivative, we define

$$h(\mathbf{t}) := K^* \frac{|\mathbf{u}|!}{(\ln 2)^{|\mathbf{u}|}} \left( \prod_{j \in \mathbf{u}} b_j \right) \prod_{j=1}^s b_j \exp\left(b_j \sqrt{-2 \log(t_j)}\right). \tag{51}$$

Similar to the analysis in Section 3.1, we apply a first-order Taylor approximation. We take the logarithm of both sides of (51):

$$\log|h(\mathbf{t})| = \sum_{j=1}^s b_j \sqrt{-2 \log(t_j)} + \log\left(K^* \frac{|\mathbf{u}|!}{(\ln 2)^{|\mathbf{u}|}} \left( \prod_{j \in \mathbf{u}} b_j \right) \prod_{j=1}^s b_j\right). \tag{52}$$

Thus, for

$$A_j = \frac{b_j}{\sqrt{-2 \log t_c^j}}, \tag{53}$$

we have

$$|h(\mathbf{t})| \leq B(\mathbf{t}) \prod_{j=1}^s (t_j)^{-A_j} \quad \mathbf{t} \notin K_{n,s}, \tag{54}$$

where

$$B(\mathbf{t}) = \left( K^* \frac{|\mathbf{u}|!}{(\ln 2)^{|\mathbf{u}|}} \left( \prod_{j \in \mathbf{u}} b_j \right) \prod_{j=1}^s b_j \right) \cdot \exp\left(\sum_{j=1}^s b_j \sqrt{\frac{-\log t_c^j}{2}}\right).$$

Similarly, we can determine  $A_j^*$  as follows:

$$A_j^* = \sqrt{\frac{\sum_{j=1}^s b_j^2}{2(\log n - \log C)}}, \tag{55}$$

$$\text{and } \max_j A_j^* = \sqrt{\frac{\sum_{j=1}^s b_j^2}{2(\log n - \log C)}}.$$

In this section, we have considered two concrete examples with unbounded variation and applied the theory developed in Section 2 to analyze their convergence rates. Consistent with the theory, the convergence rate can be improved by increasing the sample size  $n$ . However, whether we can further enhance the convergence rate by modifying the sample distribution and placing more points near the singular corners is unclear. In the next section, we discuss the effects of importance sampling.

#### 4. Importance sampling

This section provides two kinds of IS proposal distributions and analyzes their effects on the convergence rate.

##### 4.1. First proposal distribution

This section proposes a Gaussian distribution with scaled variance to distribute more samples closer to the corners. This kind of IS was studied in [28] for multivariate functions that belong to certain Sobolev spaces, where the worst-case integration error was analyzed and optimized.

Let  $g \in \{\exp \circ (\boldsymbol{\sigma}^T \Phi^{-1}), Q \circ \Phi^{-1}\} : [0, 1]^s \rightarrow \mathbb{R}$ , which are the two integrands considered in Section 3. We introduce the component-wise multiplication notation  $\odot$ , such that  $\boldsymbol{\alpha} \odot \mathbf{y} = \{\alpha_1 y_1, \alpha_2 y_2, \dots, \alpha_s y_s\} = \text{diag}(\boldsymbol{\alpha}) \mathbf{y}$  when  $\boldsymbol{\alpha}, \mathbf{y} \in \mathbb{R}^s$ . The integral of  $g$  over  $[0, 1]^s$  is

$$\begin{aligned} I(g) &= \int_{[0,1]^s} g(\mathbf{t}) d\mathbf{t} \\ &= \int_{\mathbb{R}^s} \nu(\mathbf{y}) \rho(\mathbf{y}) d\mathbf{y} \\ &= \prod_{j=1}^s \alpha_j \int_{\mathbb{R}^s} \nu(\boldsymbol{\alpha} \odot \mathbf{y}) \rho(\boldsymbol{\alpha} \odot \mathbf{y}) d\mathbf{y} \\ &= \prod_{j=1}^s \alpha_j \int_{[0,1]^s} \nu(\boldsymbol{\alpha} \odot \Phi^{-1}(\mathbf{t})) \cdot \frac{\rho(\boldsymbol{\alpha} \odot \Phi^{-1}(\mathbf{t}))}{\rho(\Phi^{-1}(\mathbf{t}))} d\mathbf{t}, \end{aligned} \tag{56}$$

where  $\nu = g \circ \Phi : \mathbb{R}^s \rightarrow \mathbb{R}$ ,  $\boldsymbol{\alpha} \in \mathbb{R}_+^s$ , and  $\rho$  is the  $s$ -dimensional standard normal distribution density. The integrand with IS  $g_{\text{IS}}$  is given by

$$\begin{aligned} g_{\text{IS}}(\mathbf{t}) &= \left( \prod_{j=1}^s \alpha_j \right) \nu(\boldsymbol{\alpha} \odot \Phi^{-1}(\mathbf{t})) \cdot \frac{\rho(\boldsymbol{\alpha} \odot \Phi^{-1}(\mathbf{t}))}{\rho(\Phi^{-1}(\mathbf{t}))} \\ &= \left( \prod_{j=1}^s \alpha_j \right) \nu(\bar{\mathbf{y}}) \cdot \prod_{j=1}^s \exp \left( -\frac{y_j^2}{2} (\alpha_j^2 - 1) \right), \end{aligned} \tag{57}$$

where we define  $\mathbf{y} = \Phi^{-1}(\mathbf{t})$  and  $\bar{\mathbf{y}} = \boldsymbol{\alpha} \odot \mathbf{y} = \boldsymbol{\alpha} \odot \Phi^{-1}(\mathbf{t})$ . The function  $g_{\text{IS}}$  no longer has the singularity at the boundaries for  $\alpha_j > 1$ ,  $j = 1, 2, \dots, s$ . Figure 4 illustrates the one-dimensional integrand with and without IS in Example 1.

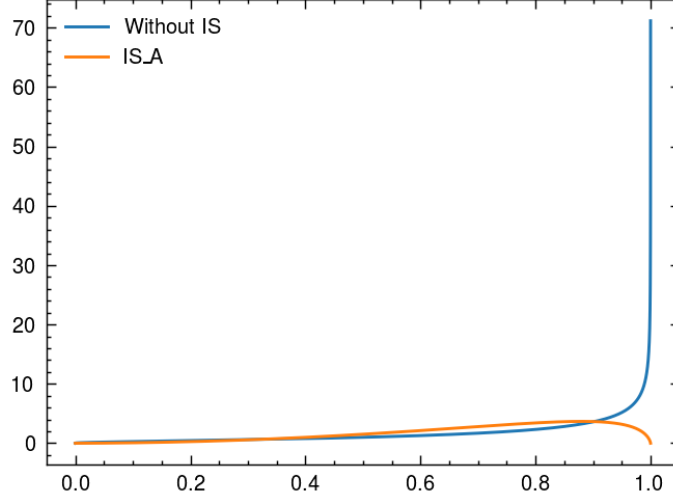


Figure 4: One-dimensional Integrands  $g$  and  $g_{\text{IS}}$  in Example 1, where  $s = 1, \sigma = 1.0, \alpha > 1$ . The "IS\_A" stands for importance sampling introduced in this section, which eliminates the singularity at the boundary.

Let us define  $\varphi(\mathbf{t}) = \prod_{j=1}^s \alpha_j \exp\left(-\frac{(\Phi^{-1}(t_j))^2}{2}(\alpha_j^2 - 1)\right)$  for the simplicity of notations. We will analyze the mixed first-order derivative  $\partial^{\mathbf{u}} g_{\text{IS}}$ . Specifically, we have

$$|\partial^{\mathbf{u}} g_{\text{IS}}(\mathbf{t})| = \left| \sum_{\mathfrak{z} \subseteq \mathbf{u}} \frac{\partial}{\partial t_{\mathbf{u}-\mathfrak{z}}} \nu(\bar{\mathbf{y}}) \cdot \partial^{\mathfrak{z}} \varphi(\mathbf{t}) \right|. \quad (58)$$

We have

$$\frac{\partial}{\partial t_{\mathbf{u}-\mathfrak{z}}} \nu(\bar{\mathbf{y}}) = \frac{\partial}{\partial \bar{\mathbf{y}}_{\mathbf{u}-\mathfrak{z}}} \nu(\bar{\mathbf{y}}) \cdot \prod_{j \in \mathbf{u}-\mathfrak{z}} \alpha_j \frac{\partial y_j}{\partial t_j}, \quad (59)$$

and

$$\partial^{\mathfrak{z}} \varphi(\mathbf{t}) = \prod_{j=1}^s \alpha_j \exp\left(-\frac{(\Phi^{-1}(t_j))^2}{2}(\alpha_j^2 - 1)\right) \cdot \prod_{k \in \mathfrak{z}} -\frac{\alpha_k^2 - 1}{2} \cdot \frac{\partial (\Phi^{-1}(t_k))^2}{\partial t_k}. \quad (60)$$

Notice that  $\binom{\mathbf{u}}{\mathfrak{z}} = 1$ , for all  $\mathfrak{z} \preceq \mathbf{u}$ . In Example 1 (i.e., when  $\nu = \exp \circ \boldsymbol{\sigma}^T$ ), we have

$$\partial^{\mathbf{u}-\mathfrak{z}} \nu(\bar{\mathbf{y}}) = \exp\left(\sum_{j=1}^s \sigma_j \bar{y}_j\right) \cdot \prod_{k \in \mathbf{u}-\mathfrak{z}} \sigma_k. \quad (61)$$

By combining equations (58) to (61), we have

$$\begin{aligned}
|\partial^{\mathbf{u}} g_{\text{IS}}(\mathbf{t})| &= \left| \sum_{\mathfrak{z} \subseteq \mathbf{u}} \frac{\partial}{\partial t_{\mathbf{u}-\mathfrak{z}}} \nu(\bar{\mathbf{y}}) \cdot \partial^{\mathbf{u}} \varphi(\mathbf{t}) \right| \\
&\leq \prod_{j=1}^s \alpha_j \exp \left( -\frac{(\Phi^{-1}(t_j))^2}{2} (\alpha_j^2 - 1) \right) \cdot \prod_{j=1}^s \exp(\sigma_j |\alpha_j \Phi^{-1}(t_j)|) \\
&\quad \cdot \sum_{\mathfrak{z} \leq \mathbf{u}} \prod_{j \in \mathbf{u}-\mathfrak{z}} \sigma_j \alpha_j \frac{\partial y_j}{\partial t_j} \cdot \prod_{k \in \mathfrak{z}} -\frac{\alpha_k^2 - 1}{2} \cdot \frac{\partial (\Phi^{-1}(t_k))^2}{\partial t_k} \\
&\approx \prod_{j=1}^s \sigma_j \alpha_j t_j^{\alpha_j^2 - 1} \cdot \exp \left( \alpha_j \sigma_j \sqrt{-2 \log(t_j)} \right) \\
&\quad \cdot \sum_{\mathfrak{z} \leq \mathbf{u}} \prod_{j \in \mathbf{s}-\mathfrak{z}} \sigma_j \alpha_j \frac{1}{t_j \sqrt{-2 \log(t_j)}} \prod_{k \in \mathfrak{z}} \frac{\alpha_k^2 - 1}{t_k},
\end{aligned} \tag{62}$$

where we have substituted  $1-t_j$  by  $t_j$  to focus on the boundary growth condition at the singularity. Before further analysis, we now analyze the derivative in Example 2.

In Example 2,  $\nu = Q$ , we apply the following upper bound of  $|\partial^{\mathbf{u}-\mathfrak{z}} Q(\bar{\mathbf{y}})|$ :

$$|\partial^{\mathbf{u}-\mathfrak{z}} Q(\bar{\mathbf{y}})| \leq \frac{|\mathbf{u}-\mathfrak{z}|!}{(\ln 2)^{|\mathbf{u}-\mathfrak{z}|}} \left( \prod_{j \in \mathbf{u}-\mathfrak{z}} b_j \right) K^* \prod_{j=1}^s \exp(b_j |\bar{y}_j|). \tag{63}$$

Combining equations (58) to (60) and (63), we obtain

$$\begin{aligned}
|\partial^{\mathbf{u}} g_{\text{IS}}(\mathbf{t})| &= \left| \sum_{\mathfrak{z} \subseteq \mathbf{u}} \partial^{\mathbf{u}-\mathfrak{z}} Q(\mathbf{t}) \cdot \partial^{\mathbf{u}} \varphi(\mathbf{t}) \right| \\
&\leq K^* \prod_{j=1}^s \alpha_j \exp \left( -\frac{(\Phi^{-1}(t_j))^2}{2} (\alpha_j^2 - 1) \right) \cdot \prod_{j=1}^s \exp(b_j |\alpha_j \Phi^{-1}(t_j)|) \\
&\quad \cdot \sum_{\mathfrak{z} \leq \mathbf{u}} \frac{|\mathbf{u}-\mathfrak{z}|!}{(\ln 2)^{|\mathbf{u}-\mathfrak{z}|}} \left( \prod_{j \in \mathbf{s}-\mathfrak{z}} b_j \right) \prod_{j \in \mathbf{u}-\mathfrak{z}} \alpha_j \frac{\partial y_j}{\partial t_j} \cdot \prod_{k \in \mathfrak{z}} -\frac{\alpha_k^2 - 1}{2} \cdot \frac{\partial (\Phi^{-1}(t_k))^2}{\partial t_k} \\
&\approx K^* \prod_{j=1}^s \alpha_j t_j^{\alpha_j^2 - 1} \cdot \exp \left( \alpha_j b_j \sqrt{-2 \log(t_j)} \right) \\
&\quad \cdot \sum_{\mathfrak{z} \leq \mathbf{u}} \frac{|\mathbf{u}-\mathfrak{z}|!}{(\ln 2)^{|\mathbf{u}-\mathfrak{z}|}} \prod_{j \in \mathbf{s}-\mathfrak{z}} b_j \alpha_j \frac{1}{t_j \sqrt{-2 \log(t_j)}} \prod_{k \in \mathfrak{z}} \frac{\alpha_k^2 - 1}{t_k},
\end{aligned} \tag{64}$$

where we use the approximation  $\Phi^{-1}(t) \approx -\sqrt{-2 \log(t)}$  and omit the term  $1/\sqrt{-2 \log t_j} = o(t_j^{-1})$ , as  $t \rightarrow 0$ . We observe that the upper bound (64) shares

similar structures with (62). We will analyze the upper bound (64) in detail and show later that the conclusions will apply to (62) of Example 1 as well.

Similar to the analysis in Section 3.1, we have

$$\exp\left(\alpha_j b_j \sqrt{-2 \log(t_j)}\right) \leq C(\mathbf{t}) \cdot (t_j)^{-B_j}, \quad (65)$$

where  $B_j = \frac{\alpha_j b_j}{\sqrt{-2 \log t_j}}$ . Notice that  $\frac{1}{t \sqrt{-2 \log(t)}} = o(t^{-1})$  as  $t \rightarrow 0$ . Thus,

$$|\partial^u g_{\text{IS}}(\mathbf{t})| \leq C \prod_{j=1}^s (t_j)^{-1+\alpha_j^2-1-B_j}. \quad (66)$$

The term  $\alpha_j^2-1-B_j$  being greater than or equal to 0 ensures the term  $\max_j A_j^* \leq 0$  in the convergence model (29), which happens when

$$\alpha_j^2 - \alpha_j \frac{b_j}{\sqrt{-2 \log t_j}} \geq 1, \quad (67)$$

which is guaranteed by  $\alpha_j > 1$  and a finite  $t_j^{-1}$  such that  $t_j^{-1} \geq \exp\left(\frac{1}{2} \left(\frac{\alpha_j b_j}{\alpha_j^2-1}\right)^2\right)$ .

For the optimality condition in Example 1 we can simply replace  $b_j$  in (67) with  $\sigma_j$ . Finite  $t_j$  for  $j = 1, \dots, s$  imply finite  $n$  (via the hyperbolic set (15)), thus the rate  $\mathcal{O}(n^{-1})$  is achievable with a finite  $n$ , in contrast to the asymptotic optimal rates in (44) and (55).

Nevertheless, modifying  $\alpha$  changes the variance of the integrand  $g_{\text{IS}}$ . Thus, we aim to determine the optimal  $\alpha^*$  by minimizing the variance of  $g_{\text{IS}}$ :

$$\text{Var}(g_{\text{IS}}) = \mathbb{E}[g_{\text{IS}}^2] - (\mathbb{E}[g_{\text{IS}}])^2, \quad (68)$$

which is equivalent to finding the minimizer for the second-order moment of  $g_{\text{IS}}$ , as  $\mathbb{E}[g_{\text{IS}}] = \mathbb{E}[g]$ :

$$\begin{aligned} \alpha^* &= \arg \min_{\alpha} \mathbb{E}[g_{\text{IS}}^2(\mathbf{t})] \\ &= \arg \min_{\alpha} \int_{[0,1]^s} \left( \prod_{j=1}^s \alpha_j \right)^2 \nu^2(\alpha \odot \Phi^{-1}(\mathbf{t})) \cdot \frac{\rho^2(\alpha \odot \Phi^{-1}(\mathbf{t}))}{\rho^2(\Phi^{-1}(\mathbf{t}))} d\mathbf{t} \\ &= \arg \min_{\alpha} \int_{\mathbb{R}^s} \left( \prod_{j=1}^s \alpha_j \right)^2 \nu^2(\alpha \odot \mathbf{y}) \cdot \frac{\rho^2(\alpha \odot \mathbf{y})}{\rho^2(\mathbf{y})} \rho(\mathbf{y}) d\mathbf{y} \\ &= \arg \min_{\alpha} \int_{\mathbb{R}^s} \left( \prod_{j=1}^s \alpha_j \right) \nu^2(\mathbf{y}) \cdot \frac{\rho^2(\mathbf{y})}{\rho^2(\frac{1}{\alpha} \odot \mathbf{y})} \rho(\frac{1}{\alpha} \odot \mathbf{y}) d\mathbf{y} \\ &= \arg \min_{\alpha} \int_{[0,1]^s} \left( \prod_{j=1}^s \alpha_j \right) \nu^2(\mathbf{y}) \cdot \frac{\rho(\mathbf{y})}{\rho(\frac{1}{\alpha} \odot \mathbf{y})} d\mathbf{t}. \end{aligned} \quad (69)$$

When the analytic solution is unavailable, we aim to find an approximate optimizer  $\bar{\alpha}$  using  $n$  samples. Specifically, we minimize the following objective function

$$\bar{\alpha} = \arg \min_{\alpha} \left( \prod_{j=1}^s \alpha_j \right) \frac{1}{n} \sum_{i=1}^n Q^2(\mathbf{y}_i) \cdot \frac{\rho(\mathbf{y}_i)}{\rho(\frac{1}{\alpha} \odot \mathbf{y}_i)}. \quad (70)$$

In practice, the number  $n$  in the pilot run does not exceed the number of simulations samples.

#### 4.2. Second proposal distribution

This section considers another IS proposal distribution. We will only analyze Example 2 for brevity, as the case for Example 1 can be derived similarly. Inspired by the beta distribution, we propose the following distribution  $\rho_{\beta} : [0, 1] \rightarrow \mathbb{R}_+$ :

$$\rho_{\beta}(t) = \begin{cases} Ct^{\beta-1} & 0 \leq t < \frac{1}{2} \\ C(1-t)^{\beta-1} & \frac{1}{2} \leq t \leq 1, \end{cases} \quad (71)$$

with the constant  $C = \beta \cdot (\frac{1}{2})^{1-\beta}$ . The reason to propose such a distribution is the ease of computing the CDF  $\Phi_{\beta} : [0, 1] \rightarrow [0, 1]$  and its inverse  $\Phi_{\beta}^{-1} : [0, 1] \rightarrow [0, 1]$ :

$$\Phi_{\beta}(t) = \begin{cases} \frac{C}{\beta} t^{\beta} & 0 \leq t < \frac{1}{2} \\ 1 - \Phi_{\beta}(1-t) & \frac{1}{2} \leq t \leq 1, \end{cases} \quad (72)$$

$$t = \Phi_{\beta}^{-1}(w) = (2w)^{\frac{1}{\beta}} \cdot \frac{1}{2} \quad \text{where } 0 \leq w < 1/2. \quad (73)$$

Next, we apply IS to compute the integral  $I(g)$ . Using the density  $\rho_{\beta}$ , we can write

$$\begin{aligned} I(g) &= \int_{[0,1]^s} g(\mathbf{t}) d\mathbf{t} \\ &= \int_{[0,1]^s} g(\mathbf{t}) \cdot \frac{\rho_{\beta}(\mathbf{t})}{\rho_{\beta}(\mathbf{t})} d\mathbf{t} \\ &= \int_{[0,1]^s} g(\Phi_{\beta}^{-1}(\mathbf{w})) \cdot \frac{1}{\rho_{\beta}(\Phi_{\beta}^{-1}(\mathbf{w}))} d\mathbf{w}. \end{aligned} \quad (74)$$

In Example 2,  $g = Q \circ \Phi^{-1}$ , and we introduce

$$g_{\text{IS}}(\mathbf{w}) = Q\left(\Phi^{-1}(\Phi_{\beta}^{-1}(\mathbf{w}))\right) \cdot \frac{1}{\rho_{\beta}(\Phi_{\beta}^{-1}(\mathbf{w}))}. \quad (75)$$

Similar to the last section, a possible choice of the parameter  $\beta$  can be determined by minimizing the second-order moment of  $g_{\text{IS}}$ :

$$\begin{aligned}\beta^* &= \arg \min_{\beta} \mathbb{E}[g_{\text{IS}}^2(\mathbf{w})] \\ &= \arg \min_{\beta} \int_{[0,1]^s} \left( \frac{g(\Phi^{-1}(\mathbf{t}))}{\rho_{\beta}(\mathbf{w})} \right)^2 \cdot \rho_{\beta}(\mathbf{w}) d\mathbf{w} \\ &= \arg \min_{\beta} \int_{[0,1]^s} \frac{g^2(\Phi^{-1}(\mathbf{w}))}{\rho_{\beta}(\mathbf{w})} d\mathbf{w}.\end{aligned}\tag{76}$$

Again, we seek an optimizer based on ensembles when the analytical solution is unavailable.

Next, we study the mixed first-order derivative of  $g_{\text{IS}}$ :

$$\left| \frac{\partial}{\partial w_u} g_{\text{IS}}(\mathbf{w}) \right| = \left| \sum_{\mathfrak{z} \subseteq u} \frac{\partial}{\partial w_{u-\mathfrak{z}}} Q\left(\Phi^{-1}(\Phi_{\beta}^{-1}(\mathbf{w}))\right) \cdot \frac{\partial}{\partial w_{\mathfrak{z}}} \varphi(\mathbf{w}) \right|,\tag{77}$$

where  $\varphi(\mathbf{w}) = \frac{1}{\rho_{\beta}(\Phi_{\beta}^{-1}(\mathbf{w}))}$ . We have

$$\frac{\partial}{\partial w_{u-\mathfrak{z}}} Q(\mathbf{w}) = \frac{\partial}{\partial \bar{y}_{u-\mathfrak{z}}} Q(\bar{\mathbf{y}}) \cdot \prod_{j \in u-\mathfrak{z}} \frac{\partial \bar{y}_j}{\partial t_j} \frac{\partial t_j}{\partial w_j}\tag{78}$$

and

$$\begin{aligned}\frac{\partial}{\partial u_{\mathfrak{z}}} \varphi(\mathbf{w}) &= \frac{\partial}{\partial u_{\mathfrak{z}}} \prod_{k=1}^s \frac{1}{\rho_{\beta_j}(\Phi_{\beta_j}^{-1}(\mathbf{w}))} \\ &= \prod_{k=1}^s \frac{1}{\beta_k} (2w_k)^{\frac{1}{\beta_k}-1} \cdot \prod_{j \in \mathfrak{z}} \frac{1-\beta_j}{\beta_j} w_j^{-1},\end{aligned}\tag{79}$$

where we define  $\bar{\mathbf{y}} = \Phi^{-1}(\mathbf{t})$  and  $\mathbf{t} = \Phi_{\beta}^{-1}(\mathbf{w})$ . We only consider the case where  $0 \leq w_j < 1/2, \forall j = 1, \dots, s$  for simplicity, as other cases can be induced by symmetry. We have

$$\frac{\partial t_j}{\partial w_j} = \frac{1}{\beta_j} (2w_j)^{\frac{1}{\beta_j}-1},\tag{80}$$

and

$$\begin{aligned}\frac{\partial \bar{y}_j}{\partial t_j} &= \frac{\partial \Phi^{-1}(t_j)}{\partial t_j} \\ &\approx -\frac{\partial \sqrt{-2 \log t_j}}{\partial t_j} \\ &= \frac{1}{t_j \sqrt{-2 \log t_j}}.\end{aligned}\tag{81}$$

Combining (63) and (78) to (81), we obtain

$$\begin{aligned}
\left| \frac{\partial}{\partial t_u} g_{\text{IS}}(\mathbf{w}) \right| &= \left| \sum_{\mathfrak{z} \subseteq u} \partial^{u-\mathfrak{z}} Q \left( \Phi^{-1}(\Phi_{\beta}^{-1}(\mathbf{w})) \right) \cdot \partial^{\mathfrak{z}} \varphi(\mathbf{w}) \right| \\
&= \left| \sum_{\mathfrak{z} \subseteq u} \frac{\partial}{\partial \bar{\mathbf{y}}_{u-\mathfrak{z}}} Q(\bar{\mathbf{y}}) \cdot \prod_{j \in u-\mathfrak{z}} \frac{\partial \bar{y}_j}{\partial t_j} \frac{\partial t_j}{\partial w_j} \cdot \frac{\partial}{\partial w_{\mathfrak{z}}} \varphi(\mathbf{w}) \right| \\
&\leq \left| \sum_{\mathfrak{z} \subseteq u} \frac{|u-\mathfrak{z}|!}{(\ln 2)^{|u-\mathfrak{z}|}} \left( \prod_{j \in u-\mathfrak{z}} b_j \right) K^* \prod_{j=1}^s \exp \left( b_j \left| \Phi^{-1} \left( (2w_j)^{\frac{1}{\beta}} \cdot \frac{1}{2} \right) \right| \right) \right| \\
&\quad \cdot \prod_{j \in u-\mathfrak{z}} \frac{\partial \bar{y}_j}{\partial t_j} \frac{\partial t_j}{\partial w_j} \cdot \prod_{j=1}^s \frac{1}{\beta_j} (2w_j)^{\frac{1}{\beta_j}-1} \cdot \prod_{k \in \mathfrak{z}} \frac{1-\beta_k}{\beta_k w_k}.
\end{aligned} \tag{82}$$

We apply the change of variable  $t_j = (2w_j)^{\frac{1}{\beta_j}} \cdot \frac{1}{2}$  for  $j = 1, \dots, s$  and continue



the analysis as follows:

$$\begin{aligned}
\left| \frac{\partial}{\partial t_u} g_{\text{IS}}(\mathbf{w}) \right| &\leq \left| \sum_{\mathfrak{z} \subseteq \mathbf{u}} \frac{|\mathbf{u} - \mathfrak{z}|!}{(\ln 2)^{|\mathbf{u} - \mathfrak{z}|}} \left( \prod_{j \in \mathbf{u} - \mathfrak{z}} b_j \right) K^* \prod_{j=1}^s \exp(b_j |\Phi^{-1}(t_j)|) \right| \\
&\cdot \prod_{j \in \mathbf{u} - \mathfrak{z}} \frac{\partial \bar{y}_j}{\partial t_j} \frac{\partial t_j}{\partial w_j} \cdot \prod_{j=1}^s \frac{1}{\beta_j} (2w_j)^{\frac{1}{\beta_j} - 1} \cdot \prod_{k \in \mathfrak{z}} \frac{1 - \beta_k}{\beta_k w_k} \\
&\approx \sum_{\mathfrak{z} \subseteq \mathbf{u}} \frac{|\mathbf{u} - \mathfrak{z}|!}{(\ln 2)^{|\mathbf{u} - \mathfrak{z}|}} \left( \prod_{j \in \mathbf{u} - \mathfrak{z}} b_j \right) K^* \prod_{j=1}^s \exp\left(b_j \sqrt{-2 \log(t_j)}\right) \\
&\cdot \prod_{j \in \mathbf{u} - \mathfrak{z}} \frac{1}{w_j \beta_j \sqrt{-2 \log(t_j)}} \cdot \prod_{j=1}^s \frac{1}{\beta_j} (2w_j)^{\frac{1}{\beta_j} - 1} \cdot \prod_{k \in \mathfrak{z}} \frac{1 - \beta_k}{\beta_k w_k} \\
&\approx \sum_{\mathfrak{z} \subseteq \mathbf{u}} \frac{|\mathbf{u} - \mathfrak{z}|!}{(\ln 2)^{|\mathbf{u} - \mathfrak{z}|}} \left( \prod_{j \in \mathbf{u} - \mathfrak{z}} b_j \right) K^* \prod_{j=1}^s \exp\left(b_j \sqrt{-2 \log(t_j)}\right) \\
&\cdot \prod_{j \in \mathbf{u} - \mathfrak{z}} \frac{2}{\beta_j \sqrt{-2 \log(t_j)}} \cdot \prod_{j=1}^s \frac{1}{\beta_j} (2w_j)^{\frac{1}{\beta_j} - 2} \cdot \prod_{k \in \mathfrak{z}} \frac{2(1 - \beta_k)}{\beta_k} \\
&= \sum_{\mathfrak{z} \subseteq \mathbf{u}} \frac{|\mathbf{u} - \mathfrak{z}|!}{(\ln 2)^{|\mathbf{u} - \mathfrak{z}|}} \left( \prod_{j \in \mathbf{u} - \mathfrak{z}} b_j \right) K^* \prod_{j=1}^s \exp\left(b_j \sqrt{-2 \log(t_j)}\right) \\
&\cdot \prod_{j \in \mathbf{u} - \mathfrak{z}} \frac{2}{\beta_j^2 \sqrt{-2 \log(t_j)}} \cdot \prod_{k \in \mathfrak{z}} \frac{2(1 - \beta_k)}{\beta_k^2} \cdot \prod_{j=1}^s (2t_j)^{1 - 2\beta_j} \\
&\leq C \prod_{j=1}^s (t_j)^{1 - 2\beta_j - B_j} \\
&= C \prod_{j=1}^s (w_j)^{\frac{1}{\beta_j} - 2 - \frac{B_j}{\beta_j}},
\end{aligned} \tag{83}$$

where in the last inequality we use,

$$\exp\left(b_j \sqrt{-2 \log(t_j)}\right) \leq C(t_j) t_j^{-B_j}$$

with  $B_j = \frac{b_j}{\sqrt{-2 \log t_j}}$ . Compared to the case without IS ( $\beta = \mathbf{1}$ ), an improved regularity of  $g_{\text{IS}}$  is achieved for  $0 < \beta_j < 1$ , as the exponent becomes larger, i.e.,  $\frac{1}{\beta_j} - 2 - \frac{B_j}{\beta_j} \geq -1 - B_j$ , when  $1 - B_j \geq 0$ . Moreover, the condition  $\frac{1}{\beta_j} - 2 - \frac{B_j}{\beta_j} \geq -1$  for  $j = 1, \dots, s$  ensures the  $\mathcal{O}(n^{-1})$  convergence rate, which requires

$$\beta_j \leq 1 - \frac{b_j}{\sqrt{-2 \log t_j}}. \tag{84}$$

Similar to the optimality condition (67) in the first proposal distribution,  $0 < \beta_j < 1$  and sufficiently large and finite  $t_j^{-1}$  for all  $j = 1, \dots, s$  and thus sufficiently large and finite  $n$  are required for the  $\mathcal{O}(n^{-1})$  convergence rate.

## 5. Numerical results

This section tests the convergence rates of the two examples we have considered, compares them with the analysis, and demonstrates how IS improves the rates.

### 5.1. Lognormal random variable expectation

We approximate the expectation of a lognormal random variable, that is,

$$\mathbb{E}[g] = \mathbb{E} \left[ \exp \left( \sum_{j=1}^s \sigma_j \xi_j \right) \right],$$

where  $\xi_j$  are i.i.d.  $\mathcal{N}(0, 1)$ . The expectation is analytically given by

$$\prod_{j=1}^s \exp \left( \frac{\sigma_j^2}{2} \right).$$

We test the convergence of the root mean squared error (RMSE) of the RQMC method using the Sobol' sequence. The RMSE for QMC is computed as follows:

$$\sqrt{\mathbb{E} \left[ \left( \frac{1}{R} \sum_{r=1}^R \frac{1}{n} \sum_{i=1}^n g(t_i \oplus \Delta_r) - \mathbb{E}[g] \right)^2 \right]} \approx \sqrt{\frac{1}{R(R-1)} \sum_{r=1}^R \left( \hat{I}_n^{(r)} - \hat{I}_{R,n} \right)^2} \quad (85)$$

where  $\hat{I}_n^{(r)} = \frac{1}{n} \sum_{i=1}^n g(t_i \oplus \Delta_r)$  and  $\hat{I}_{R,n} = \frac{1}{R} \sum_{r=1}^R \frac{1}{n} \sum_{i=1}^n g(t_i \oplus \Delta_r)$ .

With the nested uniform scrambling (Owen's scrambling) employed as the randomization, the convergence rate for the RMSE is  $\mathcal{O}(n^{-3/2+\epsilon})$  if the integrand has Lipschitz-continuous mixed first-order derivatives [38]. However, the integrand  $g$  has a singularity at 0 and thus does not have this property. In both examples presented in this work, we opt for the random linear scramble [23, 33] as the randomization. This randomization incurs lower computational cost compared to Owen's scrambling while still yielding the same variance for the RQMC estimator. (For instance, refer to Definition 6 of [40] or Section 6.12 of [10]).

Figures 5, 6, and 7 plot the convergence of the RMSE for the original integrand  $g$  and the integrand with importance sampling,  $g_{\text{IS}}$ . Each data point in these figures is RQMC estimator with the number of randomizations  $R = 30$ . Each boxplot consists of 10,000 samples. As can be observed, the IS significantly reduces the RMSE and improves the convergence rate.

Tables 1, 2, and 3 provide the measured convergence rates  $\gamma$  and the value  $(1 - \gamma)/\sqrt{\sum_{j=1}^s \sigma_j^2}$ . For the same sample size  $n$ , the convergence rate  $\gamma$  decreases as  $\sqrt{\sum_{j=1}^s \sigma_j^2}$  increases. The value  $(1 - \gamma)/\sqrt{\sum_{j=1}^s \sigma_j^2}$  exhibits similarity in magnitude for all cases in each dimension setting and increases as the dimension increases. Figure 8 plots the values  $\frac{2(1-\gamma)^2}{\sum_{j=1}^s \sigma_j^2}$  (left) and  $Cn^{-1}$  with the corresponding 95% confidence intervals. The variation within each group is also observed to be smaller than the values across groups.

Table 1: Convergence of Example 1 for dimension  $s = 1$  and standard deviation  $\sigma = \{1.0, 2.0, 3.0\}$ . The convergence rate is fitted at  $n = 2^{21}$ .

$\sigma$	Conv. Rate $\gamma$	Conv. Rate with IS	$(1 - \gamma)/\sigma$
1.0	0.875	1.888	0.125
2.0	0.719	1.340	0.141
3.0	0.582	1.088	0.139

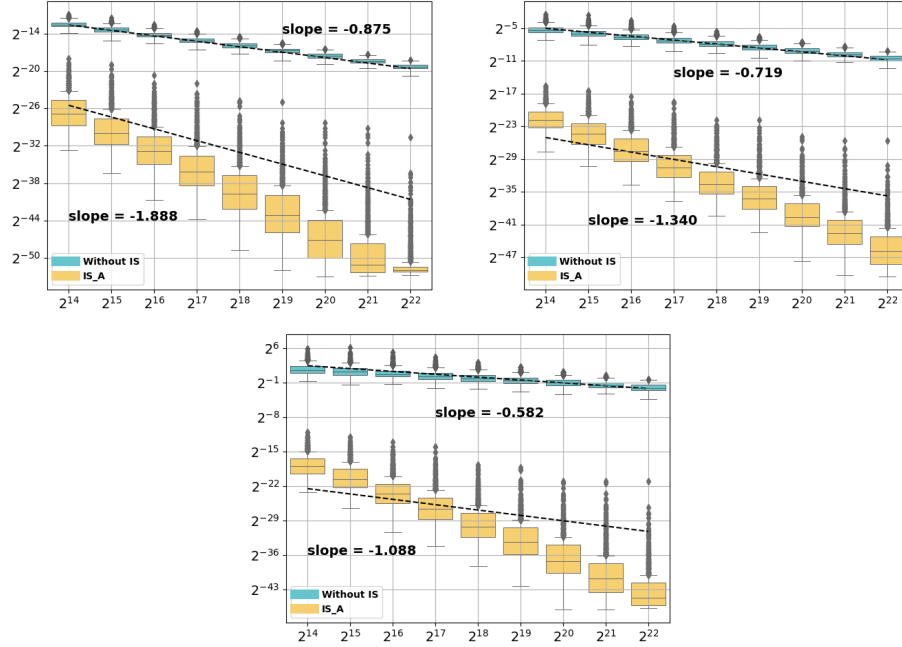


Figure 5: Example 1, the RMSE with  $s = 1$ :  $\sigma = 1.0$  (top left),  $2.0$  (top right), and  $3.0$  (bottom). Within each box, the grey horizontal line marks the median value of a total 10,000 samples. Each box extends from first quartile to the third quartile of each group and each whisker marks the 0 and 99.9 percentile. The grey diamonds denote the outliers. The boxplot settings apply to the following boxplot figures. The convergence rate is fitted at  $n = 2^{21}$ .

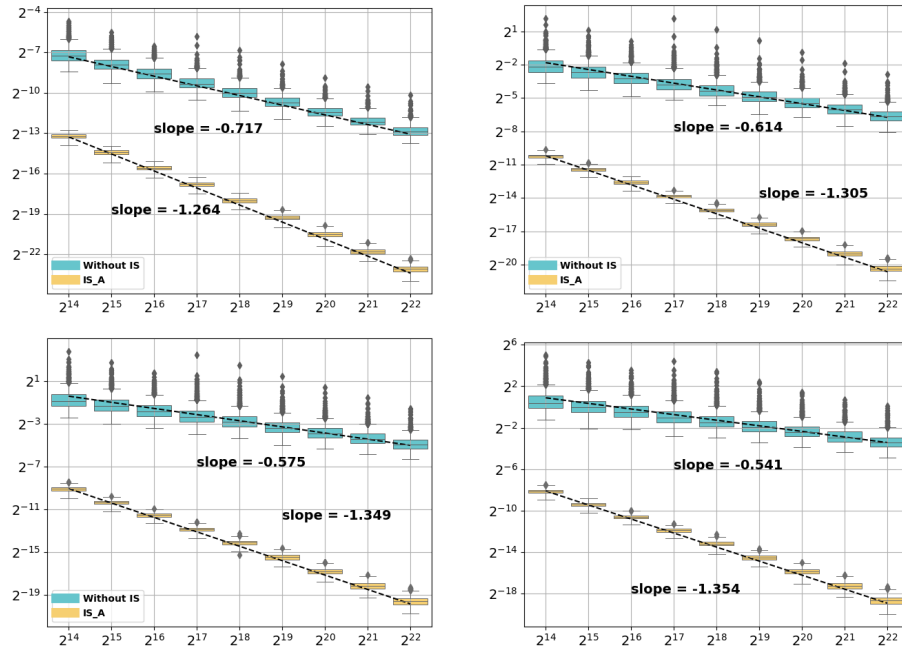


Figure 6: Example 1, the RMSE with  $s = 3$ :  $\sigma = (1.0, 1.0, 1.0)$  (top left),  $(2.0, 1.0, 1.0)$  (top right),  $(2.0, 1.4, 1.0)$  (bottom left), and  $(1.0, 1.7, 1.0)$  (bottom right). The convergence rate is fitted centered at  $n = 2^{21}$ .

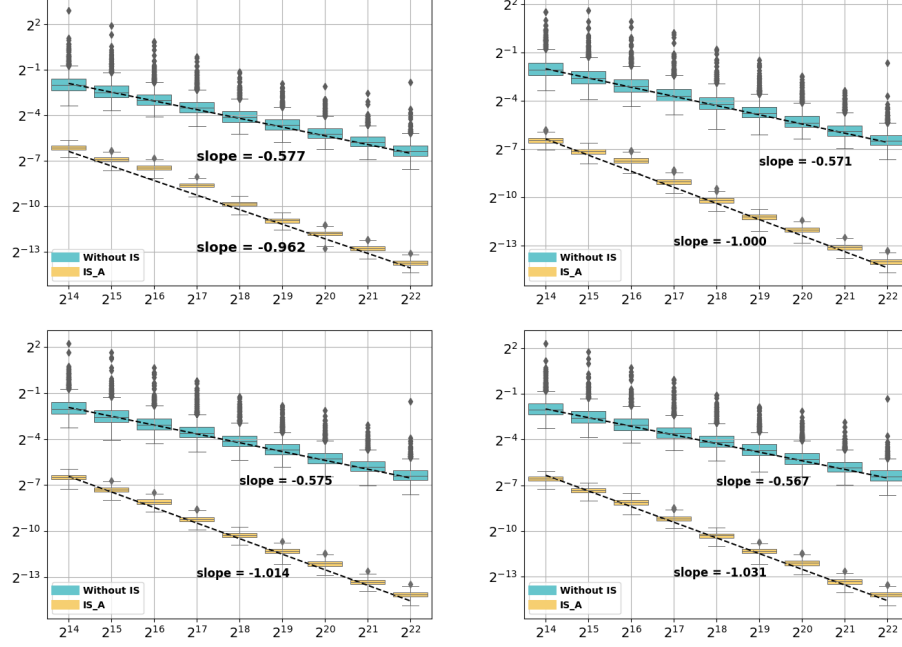


Figure 7: Example 1, the RMSE with  $s = 6$ : Case I (top left), Case II (top right), Case III (bottom left), and Case IV (bottom right). The convergence rate is fitted at  $n = 2^{21}$ .

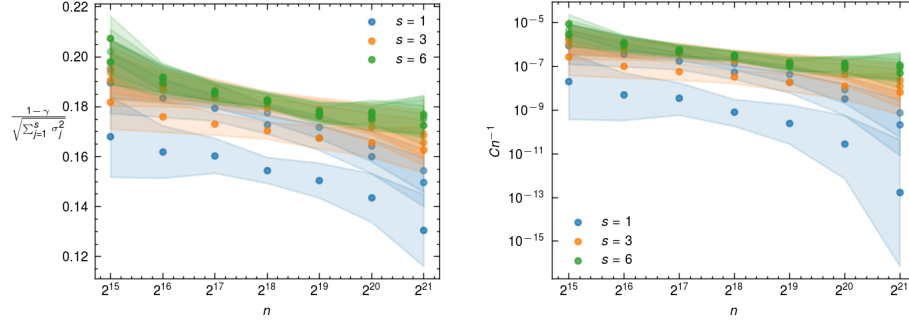


Figure 8: Example 1,  $\frac{2(1-\gamma)^2}{\sum_{j=1}^s \sigma_j^2}$  (left) and  $Cn^{-1}$  (right) against the number of samples  $n$  across various dimension and variance settings. The colors represent the dimension  $s$ , whereas each scatter point with the same color represents a unique variance setting. The shaded area is the 95% confidence interval. Both the values  $\frac{2(1-\gamma)^2}{\sum_{j=1}^s \sigma_j^2}$  (left) and  $Cn^{-1}$  decrease as the sample size increases. The values exhibit similarity in amplitude within each dimension setting.

Table 2: Convergence of Example 1, for dimension  $s = 3$  and various standard deviation settings, where the convergence rate is fitted at  $n = 2^{21}$ .

$\sigma$	Conv. Rate $\gamma$	Conv. Rate with IS	$(1 - \gamma)/\sqrt{\sum_{j=1}^s \sigma_j^2}$
(1.0, 1.0, 1.0)	0.717	1.264	0.163
(2.0, 1.0, 1.0)	0.614	1.305	0.158
(2.0, 1.4, 1.0)	0.575	1.349	0.161
(2.0, 1.7, 1.0)	0.541	1.354	0.162

Table 3: Convergence of Example 1 for dimension  $s = 6$  and various standard deviation  $\sigma$  settings, where  $\sigma_j = 1$ ,  $j = 1, \dots, s$  for Case I, and  $\sigma_j = \frac{\sqrt{6}\xi_j}{\sqrt{\sum_{j=1}^s \xi_j^2}}$ , where  $\xi_j \sim \text{Lognormal}(0, 1)$ ,  $j = 1, \dots, s$  for Cases II, III, and IV. The convergence rate is fitted at  $n = 2^{21}$ .

$\sigma$ cases	Conv. Rate $\gamma$	Conv. Rate with IS	$(1 - \gamma)/\sqrt{\sum_{j=1}^s \sigma_j^2}$
I	0.577	0.962	0.173
II	0.571	1.000	0.175
III	0.575	1.014	0.174
IV	0.567	1.031	0.178

## 5.2. Elliptic partial differential equations with lognormal coefficient

We first specify the settings of this example. The QoI is the weighted integration of the solution  $u$  over the entire domain  $\mathcal{D}$ , that is,

$$Q(u) = \int_{\mathcal{D}} g(\mathbf{x})u(\mathbf{x}; \cdot) d\mathbf{x},$$

where  $\mathcal{D} = [-1, 1]^2$ ,  $g = \rho(\cdot; \boldsymbol{\mu}, \boldsymbol{\Sigma}) * \mathbb{1}_{\mathcal{D}_0}$ ,  $*$  denotes the convolution operator,  $\mathbb{1}$  is the indicator function,  $\mathcal{D}_0 = [0.25, 0.5] \times [-0.5, -0.25] \subset \mathcal{D}$ , and  $\rho(\cdot; \boldsymbol{\mu}, \boldsymbol{\Sigma})$  represents the Gaussian density function in  $\mathbb{R}^2$  with mean  $\boldsymbol{\mu} = 0$  and covariance  $\boldsymbol{\Sigma} = \frac{1}{16}\mathbf{I}$ . The PDE problem (45a) is solved with DEAL.II [1], using the  $\mathcal{Q}_1$  finite element on a  $16 \times 16$  mesh.

Recall that the coefficient  $a$  involved in the PDE model (45) is given by,

$$a(\mathbf{x}; \omega) = \exp \left( \sum_{j=1}^s y_j \psi_j \right).$$

where the basis  $\{\psi_j\}$  are the eigenfunctions to the following Matérn covariance kernel:

$$C(h) = \frac{1}{2^{\nu-1}\Gamma(\nu)} \left( \sqrt{2\nu} \frac{h}{r} \right)^{\nu} K_{\nu} \left( \sqrt{2\nu} \frac{h}{r} \right), \quad (86)$$

where we chose  $\nu = 4.5$  and  $r = 1$ . In addition,  $\Gamma$  is the Gamma function, and  $K_{\nu}$  is the modified Bessel function of the second kind. Let  $\lambda_{j,p}$  and  $\theta_{j,p}$  be the Fourier coefficients and trigonometric functions in the Fourier expansion

of the covariance kernel  $C$  on an extended domain  $\mathcal{D}_p = [-\gamma, \gamma]^d$ , respectively, with  $d = 2$ . The extension is needed to ensure the positivity of the Fourier coefficients  $\lambda_{j,p}$  [3]. We let

$$\begin{aligned}\psi_{j,p} &= \lambda_{j,p} \theta_{j,p} \\ \psi_j &= \psi_{j,p}|_{\mathcal{D}}.\end{aligned}\tag{87}$$

Apart from the trigonometric-basis expansions, we also apply Meyer wavelet functions to construct the basis  $\psi_j$  (for a detailed analysis and instructions, see Section 4 in [3]).

To validate the proposed convergence model (55), we also considered the following coefficient:

$$a(\mathbf{x}; \omega) = \exp \left( \sum_{j=1}^s y_j \sigma_j \psi_j \right), \tag{88}$$

where we generated six samples of  $\sigma$  within each dimension setting. In the first sample,  $\sigma = \mathbf{1}$ . In the second and third samples,  $\sigma_j$  are i.i.d. sampled from the uniform distribution  $U[1, 2]$ . In the last three samples, the  $\sigma$  values of the first three cases are multiplied component-wise by 2. Figure 9 plots the deteriorated rate  $1 - \gamma$  against  $\sqrt{\sum_{j=1}^s \sigma_j^2 b_j^2}$ . The convergence rate is measured between  $2^6$  and  $2^{15}$  number of samples, with one RQMC estimator of  $R = 30$  randomizations. In all considered cases, the rate  $1 - \gamma$  exhibits an almost linear dependence on  $\sqrt{\sum_{j=1}^s \sigma_j^2 b_j^2}$ . Unlike Example 1, the effect of dimensions on the convergence rates is not obvious in both cases, which was unexpected because the QMC points quality deteriorates in higher dimensions. One possible reason for this observation lies in Equation (49), where we applied the upper bounds for  $Q$  and its derivatives, which conceals the effective dimension.

Figure 10 compares the  $L^\infty$  norm of the basis  $\psi_{j,p}$  and  $\psi_j$  between trigonometric and wavelet-type bases. The trigonometric basis is optimal in approximating the random field in the  $L^2$  sense. However, the basis  $L^\infty$  norm, which appears in the convergence model (55) and (29) is the primary interest. Ideally,  $\|\psi_j\|_{L^\infty(\mathcal{D})}$  is desired to converge fast as  $j$  increases to reduce the effective dimension. In the nonasymptotic QMC convergence model for elliptic PDEs (55), the value  $\sum_{j=1}^s b_j^2$  is expected to be small for a fixed dimension  $s$ . We observed that the values  $b_j$  of the wavelet-type basis in the plotted range are smaller than those of the trigonometric basis. The localization properties of the wavelet-type basis make it even more favorable when the function  $\psi_{j,p}$  is restricted on  $\mathcal{D}$  since  $\|\psi_j\|_{L^\infty(\mathcal{D})} \leq \|\psi_{j,p}\|_{L^\infty(\mathcal{D}_p)}$ .

Figure 11 plots the convergence of the RMSE for the original integrand  $g$  and the integrand with IS  $g_{\text{IS}}$ , where the wavelet-type basis is used for two variance settings and two dimension settings. In all cases, both types of IS improve the integrand regularity, reducing the RMSE and improving the convergence rate. Furthermore, the effectiveness of the IS is more significant when the dimension is smaller, as IS has more limitations in higher dimensions to not increase the

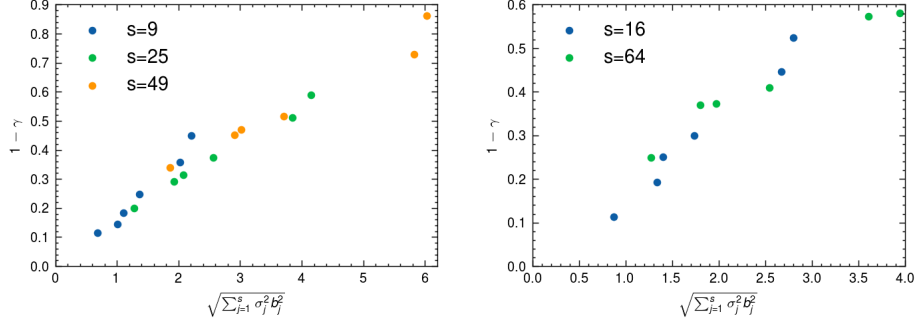


Figure 9: Example 2, the value  $(1 - \gamma)$  against  $\sqrt{\sum_{j=1}^s \sigma_j^2 b_j^2}$  for using the Fourier basis (left) and wavelet-type basis (right) across various dimension and variance settings. The colors represent the dimension  $s$ , whereas each scatter point with the same color represents a unique variance setting. The dimension-independent effect is observed in the convergence rate in both cases.

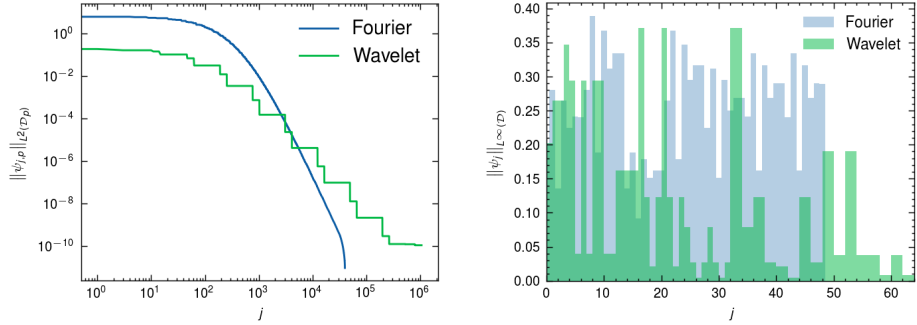


Figure 10: Example 2, a comparison of the  $L^2$  norms  $\|\psi_{j,p}\|_{L^2(\mathcal{D}_p)}$  and  $L^\infty$  norms  $\|\psi_j\|_{L^\infty(\mathcal{D})}$  between the Fourier basis and wavelet-type basis.



variance. Moreover, when the original integrand has a larger  $\sigma^2$  the IS works better because  $\alpha_j$  in (66) becomes larger and  $\beta_j$  in (83) becomes smaller.

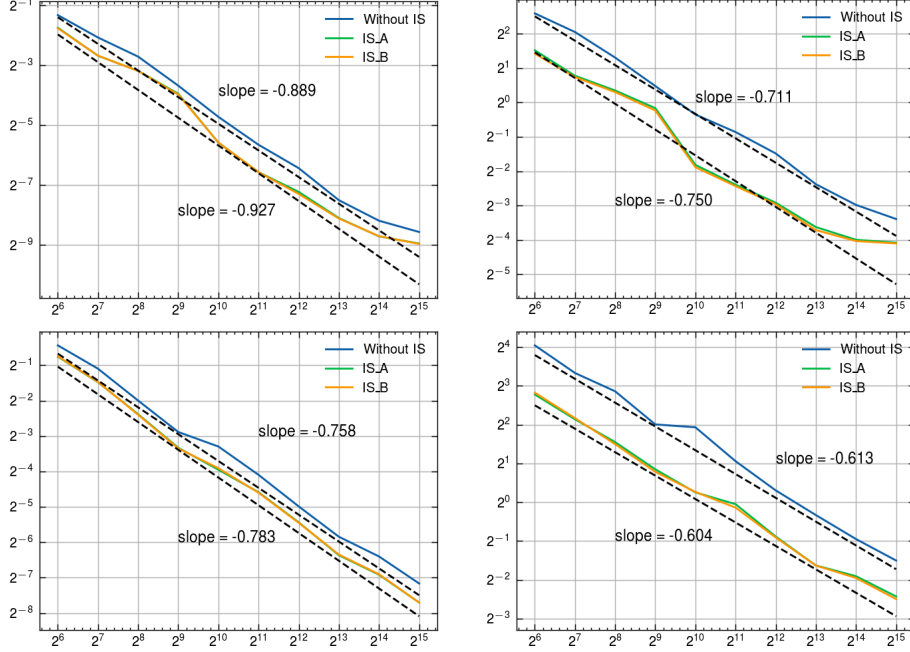


Figure 11: Example 2, the root mean squared error with and without two types of IS for  $s = 16$  (top),  $s = 64$  (bottom) with  $\sigma = 1$  (left) and  $\sigma = 2$  (right). The fitted convergence rate is marked in the figure. The random coefficient  $a$  is expressed using the wavelet-type basis.

## 6. Conclusion

In this work, we study the nonasymptotic QMC convergence rate model for functions with finite-dimensional inputs. Specifically, we focus on the expectation of a lognormal random variable and an elliptic PDE problem characterized by lognormal coefficients. Drawing upon the hyperbolic set  $K_{n,s}$  introduced in the work of Owen [39], we subdivided the integration domain. This division allowed us to split the QMC integration error into two distinct contributions, namely:  $2 \int_{[0,1]^s - K_{n,s}} |g - \tilde{g}|$  and  $\mathbb{E}[D_n^*(t_1, \dots, t_n)] V_{HK}(\tilde{g})$ . This method replaces the right-hand side of the Koksma–Hlawka inequality  $V_{HK}(g) D_n^*(\mathcal{P})$ , which is infinite for the unbounded functions considered in this work, with two finite terms.

Our primary contribution through this work has been deriving an upper bound for the integrand derivative via an optimization problem, denoted as (23). With this in place, we applied it within the convergence model, culminating in deriving the nonasymptotic QMC convergence rate model. In our quest to verify

the proposed model, we presented numerical examples for the two problems above. Moreover, the analytical procedures delineated here can find relevance in varied integration challenges, one notable instance being the option pricing problem within financial scenarios.

In addition to the above, our work also involved applying two IS distributions, leading us to evaluate their potential to enhance integrand regularity. Notably, despite the distinct support of these distributions, their influence on the integrand appeared broadly analogous.

However, there remain areas that we have not explored in depth. For instance, we have yet to derive the constant  $C$  within the hyperbolic set. Delving into its dependence on dimensionality and integrand characteristics could be a promising trajectory for subsequent studies. Moreover, future inquiries could also encompass the random field’s truncation error, where wavelets demonstrate a superior edge over the trigonometric basis, as indicated in [2]. Furthermore, examining a multilevel setting with adaptivity, as hinted at in [8], could be beneficial.

Lastly, it is worth noting our choice to employ the Sobol’ sequence instead of exploring weighted spaces or designing lattice rules (e.g., [30], [17]). The latter could reduce the worst-case integration error for specific function spaces, potentially leading to a dimension-independent outcome given certain conditions. This combination of lattice rules and nonasymptotic analysis remains a compelling avenue for future exploration.

## 7. Acknowledgement

This publication is based on work supported by the Alexander von Humboldt Foundation and the King Abdullah University of Science and Technology (KAUST) office of sponsored research (OSR) under Award No. OSR-2019-CRG8-4033. This work utilized the resources of the Supercomputing Laboratory at King Abdullah University of Science and Technology (KAUST) in Thuwal, Saudi Arabia. The authors thank Christian Bayer, Fabio Nobile and Erik von Schwerin for fruitful discussions. We are also grateful to Arved Bartuska and Michael Samet for proofreading this manuscript. Their suggestions significantly improve the paper’s readability. We acknowledge the use of the following open-source software packages: `deal.II` [1].

## References

- [1] D. ARNDT, W. BANGERTH, B. BLAIS, T. C. CLEVINGER, M. FEHLING, A. V. GRAYVER, T. HEISTER, L. HELTAI, M. KRONBICHLER, M. MAIER, P. MUNCH, J.-P. PELTERET, R. RASTAK, I. THOMAS, B. TURCK SIN, Z. WANG, AND D. WELLS, *The deal.II library, version 9.2*, Journal of Numerical Mathematics, 28 (2020), pp. 131–146.
- [2] M. BACHMAYR, A. COHEN, R. DEVORE, AND G. MIGLIORATI, *Sparse polynomial approximation of parametric elliptic PDEs. Part II: lognormal*

- coefficients*, ESAIM: Mathematical Modelling and Numerical Analysis, 51 (2017), pp. 341–363.
- [3] M. BACHMAYR, A. COHEN, AND G. MIGLIORATI, *Representations of Gaussian random fields and approximation of elliptic PDEs with lognormal coefficients*, Journal of Fourier Analysis and Applications, 24 (2018), pp. 621–649.
  - [4] C. BAYER, C. BEN HAMMOUDA, AND R. TEMPONE, *Numerical smoothing with hierarchical adaptive sparse grids and quasi-Monte Carlo methods for efficient option pricing*, Quantitative Finance, 23 (2023), pp. 209–227.
  - [5] C. BAYER, C. B. HAMMOUDA, A. PAPAPANTOLEON, M. SAMET, AND R. TEMPONE, *Optimal damping with hierarchical adaptive quadrature for efficient Fourier pricing of multi-asset options in Lévy models*, ArXiv, abs/2203.08196 (2022).
  - [6] C. BAYER, C. B. HAMMOUDA, AND R. TEMPONE, *Numerical smoothing and hierarchical approximations for efficient option pricing and density estimation*, arXiv: Computational Finance, (2020).
  - [7] C. BAYER, M. SIEBENMORGEN, AND R. TEMPONE, *Smoothing the payoff for efficient computation of basket option prices*, Quantitative Finance, 18 (2016), pp. 491–505.
  - [8] J. BECK, Y. LIU, E. VON SCHWERIN, AND R. TEMPONE, *Goal-oriented adaptive finite element multilevel Monte Carlo with convergence rates*, Computer Methods in Applied Mechanics and Engineering, 402 (2022), p. 115582.
  - [9] R. E. CAFLISCH, W. J. MOROKOFF, AND A. B. OWEN, *Valuation of mortgage backed securities using Brownian bridges to reduce effective dimension*, vol. 24, Department of Mathematics, University of California, Los Angeles, 1997.
  - [10] J. DICK, F. Y. KUO, AND I. H. SLOAN, *High-dimensional integration: the quasi-monte carlo way*, Acta Numerica, 22 (2013), pp. 133–288.
  - [11] J. DICK AND F. PILlichshammer, *Digital nets and sequences: discrepancy theory and quasi-Monte Carlo integration*, Cambridge University Press, 2010.
  - [12] G. Y. DONG AND C. LEMIEUX, *Dependence properties of scrambled Halton sequences*, Mathematics and Computers in Simulation, 200 (2022), pp. 240–262.
  - [13] M. GERBER AND N. CHOPIN, *Sequential quasi Monte Carlo*, Journal of the Royal Statistical Society: Series B (Statistical Methodology), 77 (2015), pp. 509–579.

- [14] A. D. GILBERT, F. Y. KUO, AND I. H. SLOAN, *Preintegration is not smoothing when monotonicity fails*, in Advances in Modeling and Simulation: Festschrift for Pierre L'Ecuyer, Springer, 2022, pp. 169–191.
- [15] E. GOBET, M. LERASLE, AND D. MÉTIVIER, *Mean estimation for randomized quasi Monte Carlo method*, (2022).
- [16] T. GODA AND P. L'ECUYER, *Construction-free median quasi-Monte Carlo rules for function spaces with unspecified smoothness and general weights*, SIAM Journal on Scientific Computing, 44 (2022), pp. A2765–A2788.
- [17] I. G. GRAHAM, F. Y. KUO, J. A. NICHOLS, R. SCHEICHL, C. SCHWAB, AND I. H. SLOAN, *Quasi-Monte Carlo finite element methods for elliptic PDEs with lognormal random coefficients*, Numerische Mathematik, 131 (2015), pp. 329–368.
- [18] M. GRIEBEL, F. KUO, AND I. SLOAN, *The smoothing effect of integration in  $\mathbb{R}^d$  and the ANOVA decomposition*, Mathematics of Computation, 82 (2013), pp. 383–400.
- [19] A. GRIEWANK, F. Y. KUO, H. LEÖVEY, AND I. H. SLOAN, *High dimensional integration of kinks and jumps—smoothing by preintegration*, Journal of Computational and Applied Mathematics, 344 (2018), pp. 259–274.
- [20] Z. HE AND X. WANG, *On the convergence rate of randomized quasi-Monte Carlo for discontinuous functions*, SIAM Journal on Numerical Analysis, 53 (2015), pp. 2488–2503.
- [21] Z. HE, Z. ZHENG, AND X. WANG, *On the error rate of importance sampling with randomized quasi-Monte Carlo*, arXiv preprint arXiv:2203.03220, (2022).
- [22] L. HERRMANN AND C. SCHWAB, *QMC integration for lognormal-parametric, elliptic PDEs: local supports and product weights*, Numerische Mathematik, 141 (2019), pp. 63–102.
- [23] H. S. HONG AND F. J. HICKERNELL, *Algorithm 823: Implementing scrambled digital sequences*, ACM Transactions on Mathematical Software (TOMS), 29 (2003), pp. 95–109.
- [24] J. IMAI AND K. S. TAN, *A general dimension reduction technique for derivative pricing*, Journal of Computational Finance, 10 (2006), p. 129.
- [25] ———, *Pricing derivative securities using integrated quasi-Monte Carlo methods with dimension reduction and discontinuity realignment*, SIAM Journal on Scientific Computing, 36 (2014), pp. A2101–A2121.
- [26] X. JIN AND A. X. ZHANG, *Reclaiming Quasi-Monte Carlo efficiency in portfolio value-at-risk simulation through Fourier transform*, Management Science, 52 (2006), pp. 925–938.

- [27] Y. KAZASHI, *Quasi-Monte Carlo integration with product weights for elliptic pdes with log-normal coefficients*, IMA Journal of Numerical Analysis, 39 (2019), pp. 1563–1593.
- [28] P. KRITZER, F. PILLICHSHAMMER, L. PLASKOTA, AND G. W. WASILKOWSKI, *On efficient weighted integration via a change of variables*, Numerische Mathematik, 146 (2018), pp. 545–570.
- [29] F. Y. KUO AND D. NUYENS, *A practical guide to quasi-Monte Carlo methods*, (2016).
- [30] F. Y. KUO, C. SCHWAB, AND I. H. SLOAN, *Quasi-Monte Carlo finite element methods for a class of elliptic partial differential equations with random coefficients*, SIAM J. Numer. Anal., 50 (2012), pp. 3351–3374.
- [31] S. LIU AND A. B. OWEN, *Preintegration via active subspace*, SIAM Journal on Numerical Analysis, 61 (2023), pp. 495–514.
- [32] P. L’ECUYER, *Randomized quasi-Monte Carlo: An introduction for practitioners*, Springer, 2018.
- [33] J. MATOUŠEK, *On the  $L_2$ -discrepancy for anchored boxes*, Journal of Complexity, 14 (1998), pp. 527–556.
- [34] W. J. MOROKOFF AND R. E. CAFLISCH, *Quasi-random sequences and their discrepancies*, SIAM Journal on Scientific Computing, 15 (1994), pp. 1251–1279.
- [35] J. A. NICHOLS AND F. Y. KUO, *Fast CBC construction of randomly shifted lattice rules achieving  $\mathcal{O}(n^{-1+\delta})$  convergence for unbounded integrands over  $\mathbb{R}^s$  in weighted spaces with POD weights*, Journal of Complexity, 30 (2014), pp. 444–468.
- [36] H. NIEDERREITER, *Random number generation and quasi-Monte Carlo methods*, SIAM, 1992.
- [37] D. OUYANG, X. WANG, AND Z. HE, *Quasi-Monte Carlo for unbounded integrands with importance sampling*, arXiv preprint arXiv:2310.00650, (2023).
- [38] A. B. OWEN, *Scrambling Sobol’ and Niederreiter–Xing points*, Journal of complexity, 14 (1998), pp. 466–489.
- [39] A. B. OWEN, *Halton sequences avoid the origin*, SIAM Review, 48 (2006), pp. 487–503.
- [40] A. B. OWEN, *Local antithetic sampling with scrambled nets*, The Annals of Statistics, (2008), pp. 2319–2343.
- [41] A. B. OWEN, *Monte Carlo theory, methods and examples*, 2013.

- [42] A. B. OWEN, *A randomized Halton algorithm in R*, arXiv preprint arXiv:1706.02808, (2017).
- [43] Z. PAN AND A. OWEN, *Super-polynomial accuracy of one dimensional randomized nets using the median of means*, Mathematics of Computation, 92 (2023), pp. 805–837.
- [44] A. PAPAGEORGIOU, *The Brownian bridge does not offer a consistent advantage in quasi-Monte Carlo integration*, Journal of Complexity, 18 (2002), pp. 171–186.
- [45] J. K. PATEL AND C. B. READ, *Handbook of the normal distribution*, vol. 150, CRC Press, 1996.
- [46] I. PINELIS, *Exact lower and upper bounds on the incomplete gamma function*, arXiv preprint arXiv:2005.06384, (2020).
- [47] I. H. SLOAN AND H. WOŹNIAKOWSKI, *When are quasi-Monte Carlo algorithms efficient for high dimensional integrals?*, Journal of Complexity, 14 (1998), pp. 1–33.
- [48] I. SOBOLOV, *Calculation of improper integrals using equidistributed sequences*, Doklady Akademii Nauk SSSR, 210 (1973), pp. 278–281.
- [49] X. WANG, *Dimension reduction techniques in quasi-Monte Carlo methods for option pricing*, INFORMS Journal on Computing, 21 (2009), pp. 488–504.
- [50] X. WANG AND K.-T. FANG, *The effective dimension and quasi-Monte Carlo integration*, Journal of Complexity, 19 (2003), pp. 101–124.
- [51] X. WANG AND I. H. SLOAN, *Why are high-dimensional finance problems often of low effective dimension?*, SIAM Journal on Scientific Computing, 27 (2005), pp. 159–183.
- [52] ———, *Low discrepancy sequences in high dimensions: How well are their projections distributed?*, Journal of Computational and Applied Mathematics, 213 (2008), pp. 366–386.
- [53] ———, *Quasi-Monte Carlo methods in financial engineering: An equivalence principle and dimension reduction*, Operations Research, 59 (2011), pp. 80–95.
- [54] X. WANG AND K. S. TAN, *Pricing and hedging with discontinuous functions: Quasi-Monte Carlo methods and dimension reduction*, Management Science, 59 (2013), pp. 376–389.
- [55] C. WENG, X. WANG, AND Z. HE, *Efficient computation of option prices and Greeks by quasi-Monte Carlo method with smoothing and dimension reduction*, SIAM Journal on Scientific Computing, 39 (2017), pp. B298–B322.

- [56] J. WIART, C. LEMIEUX, AND G. Y. DONG, *On the dependence structure and quality of scrambled  $(t, m, s)$ -nets*, Monte Carlo Methods and Applications, 27 (2019), pp. 1 – 26.